Journal of Contaminant Hydrology 244 (2022) 103922

Contents lists available at ScienceDirect

Journal of Contaminant Hydrology

journal homepage: www.elsevier.com/locate/jconhyd

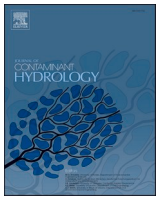

A two-way coupled model for the co-transport of two different colloids in porous media

N. Seetha [a,*], S. Majid Hassanizadeh [b,c]

[a] Department of Civil Engineering, Indian Institute of Technology Hyderabad, Telangana 502285, India
[b] Stuttgart Center for Simulation Science (SIMTECH), Integrated Research Training Group SFB 1313, Stuttgart University, Germany
[c] Department of Earth Sciences, Utrecht University, 3584, CB, Utrecht, The Netherlands

ARTICLE INFO

Keywords:
Co-transport
Colloids
Porous media
Heteroaggregation
Two-way coupled model

ABSTRACT

Models for the co-transport of two different colloids commonly assume a one-way coupling. This is because often a large colloid and small colloid are involved. Therefore, they assume that the spread of smaller colloid is affected by the transport of larger colloids, but not the other way around. However, a number of studies have shown that this assumption is not valid, even for large and small colloids. Therefore, in this study, a two-way coupled model is developed to simulate the co-transport of two different colloids in porous media and their effect on each other. We have considered the interactions of the two colloids with the grain surface, kinetics of heteroaggregation (of the two colloids), and heteroaggregate deposition onto the grain surface. We assumed a first-order kinetic model to represent heteroaggregate formation and its deposition on the grain surface. The model is evaluated by fitting the experimental data reported in four different papers from the literature on the co-transport of clay colloids and viruses, bacteria and graphene oxide nanoparticles, and clay colloids and graphene oxide nanoparticles. The model performance is compared with the commonly-used one-way coupled model. The two-way coupled model is found to satisfactorily simulate most of the experimental conditions reported in the above papers, except for the co-transport of montmorillonite–adenovirus, and *Staphylococcus aureus*- graphene oxide nanoparticles.

1. Introduction

Predicting the transport behaviour of colloidal contaminants such as pathogenic microorganisms and engineered nanoparticles in the subsurface is essential for the assessment of groundwater contamination risks (Ron and Johnson, 2020; Schijven and Hassanizadeh, 2002; Schijven et al., 2010), to estimate the safe distance of drinking water wells from (potential) contamination sources (Schijven et al., 2006), to decide on the degree of treatment required before supplying the groundwater for drinking purposes (Schijven et al., 1999, 2000), and to remediate contaminated groundwater (Malakar and Snow, 2020). It is found that the release pathways of colloidal contaminants, including point sources (such as deep well injection for bioremediation) and distributed sources (e.g., rainfall events, landfills, irrigation activities), have a significant impact on their fate and transport in the subsurface (Mahmoudi et al., 2020). There are also colloids that do not really pose any groundwater quality threats, but may act as carriers of contaminating colloids. For example, natural colloids, such as clays, are abundant in the subsurface and have been found to facilitate the transport of contaminants such as biocolloids and engineered nanoparticles (Cai et al., 2014; Vasiliadou and Chrysikopoulos, 2011; Walshe et al., 2010). So, it is very important to study the co-transport of two different colloids.

A number of experimental studies have investigated the co-transport of multiple colloids in porous media including clay and bacteria (Vasiliadou and Chrysikopoulos, 2011; Yang et al., 2012), clay and viruses (Jin et al., 2000; Syngouna and Chrysikopoulos, 2013; Syngouna et al., 2017; Walshe et al., 2010), clay and engineered nanoparticles (Bayat et al., 2015; Cai et al., 2014; Chrysikopoulos et al., 2017), clay and plastic particles (Li et al., 2020), silica nanoparticles and viruses (Qin et al., 2020), bacteria and engineered nanoparticles (Cai et al., 2016; Georgopoulou et al., 2020), viruses and engineered nanoparticles (Syngouna et al., 2017), iron oxide particles and engineered nanoparticles (Wang et al., 2021), plastic particles and engineered nanoparticles (Cai et al., 2019; Dong et al., 2019), and a mixture of engineered nanoparticles (Cai et al., 2013; Kumari et al., 2015). Experimental results from these studies indicate that the transport behaviors of both colloids are different when they are co-present as

* Corresponding author.
E-mail address: seetha@ce.iith.ac.in (N. Seetha).

https://doi.org/10.1016/j.jconhyd.2021.103922
Received 30 October 2020; Received in revised form 4 October 2021; Accepted 13 November 2021
Available online 16 November 2021

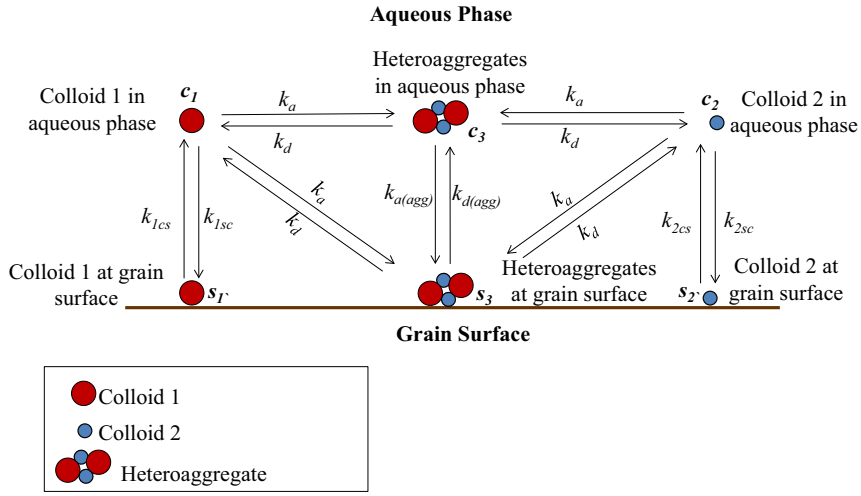

Fig. 1. Conceptual representation of various interactions among colloids and grain surface in porous media.

compared to their individual transport. Also, the co-presence of a different colloid can either increase or decrease the transport of bacteria, viruses, and engineered nanoparticles, depending on the interactions of the two colloids with the grain surface, competition between the two colloids to find deposition sites on the grain surface, heteroaggregation of colloids in the aqueous phase and at the grain surface, and deposition of heteroaggregates on the grain surface.

The experimental studies involving the co-transport of micrometer- and nanometer-sized particles (e.g., clay-bacteria, clay-viruses, clay-engineered nanoparticles, and bacteria-engineered nanoparticles) revealed a greater retention of both particles in porous media when they are co-present together than their individual transport behaviour. The mechanisms that have been proposed for the increased retention are the formation of heteroaggregates (aggregates of two different colloids) in the aqueous and solid phases, and the co-deposition of the two colloids to the grain surface (Chrysikopoulos et al., 2017; Georgopoulou et al., 2020; Li et al., 2019; Yang et al., 2012). Sotirelis and Chrysikopoulos (2017), Georgopoulou et al. (2020), and Vasiliadou and Chrysikopoulos (2011) found from batch experiments that the heteroaggregation of graphene oxide nanoparticles-kaolinite, graphene oxide nanoparticles-montmorillonite, and *Pseudomonas putida*-kaolinite, respectively, can be described using a pseudo second-order kinetic model. Also, heteroaggregates (e.g., iron oxide-plastic particles, nanoplastics-fullerene, micron sized plastic particles-kaolinite and ZnO-CuO) are found to have different surface charges, and hence may interact differently with the solid surface than the individual colloids (Dong et al., 2019; Li et al., 2019, 2020; Parsai and Kumar, 2019). Therefore, it is important to account for the kinetics of heteroaggregation and its deposition on the grain surface to simulate the co-transport of multiple colloids in porous media.

A one-dimensional one-way coupled mathematical model describing the co-transport of clay particles and bacteria under saturated conditions was developed by Vasiliadou and Chrysikopoulos (2011) and was used by Seetha et al. (2015) to describe the co-transport of viruses and clay colloids. This model has been further extended to three dimensions by Katzourakis and Chrysikopoulos (2014, 2015). The above models assume that the presence of attached bacteria (or viruses) on the clay particle surface will not affect the transport behaviour of clay colloids. This model does not account for the kinetics of heteroaggregate formation and does not distinguish between the interaction of clay colloids and clay-bacteria heteroaggregate with the grain surface. Thus, clay colloid transport equations were decoupled from the bacteria (or virus) transport equations. This would imply that the individual clay colloids and heteroaggregates of clay-bacteria (or clay-viruses) should have the same transport behaviour, and the values of attachment and detachment rate coefficients for clay colloids obtained from experiments with clay colloids only should be applicable in modelling co-transport experiments. However, results of simulations by Seetha et al. (2015) showed that this is not the case; for a satisfactory fit of co-transport experimental data using one-way coupled model, they had to use significantly different values for attachment and detachment rate coefficients of clay colloids during co-transport than the values obtained from clay colloids-only transport experiments. This means that transport behaviour of both clays and bacteria (or viruses) are different when they are co-present as compared to their individual transport. This implies that a two-way coupled model describing the co-transport of two different colloids is needed.

The objective of this study is to develop a 1D two-way coupled model to simulate the co-transport of two different colloids in saturated porous media. The extension to three dimensions is trivial. The model accounts for deposition of both colloids on the grain surface, kinetics of heteroaggregation using a first-order model, and deposition of heteroaggregates onto the grain surface. This is the first study where the co-transport of two different colloids in porous media is modelled by accounting for the heteroaggregation kinetics. The developed model is evaluated by fitting experimental data from four different studies reported in the literature. The model performance is also compared with that of a simple one-way coupled model.

2. Two-way coupled mathematical model

2.1. Model development

In this study, we consider the co-transport of two different colloids. Fig. 1 shows the various forms of colloids and the interactions among colloids and with grain surface. Here, we have shown a large colloid (colloid 1) and a small one (colloid 2) because that is the case in many applications, as well as in the four experimental studies that we have simulated here. However, the model developed here and governing equations that are presented below are valid for any size of colloids. Both colloids 1 and 2 can exist in free form in aqueous phase and as immobile colloids attached to solid surface. In addition, colloids 1 and 2 undergo heteroaggregation. Heteroaggregates exists in two different forms: in mobile form in aqueous phase and in immobile form attached to solid surface. Assumptions involved in the model development are: (a) the formation of the heteroaggregates is described using a first-order reversible kinetic model, (b) the rate coefficients for attachment of colloid 1 to colloid 2 is the same as that of colloid 2 to colloid 1, (c) the

properties of heteroaggregates are different from that of individual colloids, and (d) the deposition of heteroaggregates onto grain surface is described using a first-order reversible kinetic model.

The governing equation for the transport of colloid 1 is given below. Colloid 1 may be present in the aqueous phase (with concentration c_1), can be adsorbed to the grain surface (with mass fraction s_1), can form part of a free heteroaggregate in the aqueous phase (with concentration $(1 - s_m)c_3$), or can be part of a heteroaggregate attached to the solid phase (with mass fraction $(1 - s_{im})$). Then we have:

$$\theta\frac{\partial c_1}{\partial t}+\rho_b\frac{\partial s_1}{\partial t}+\theta\frac{\partial(1-s_m)c_3}{\partial t}+\rho_b\frac{\partial(1-s_{im})s_3}{\partial t} = \theta {D_L}^1\frac{\partial^2 c_1}{\partial z^2}+\theta {D_L}^1\frac{\partial^2(1-s_m)c_3}{\partial z^2}-v_1\theta\frac{\partial c_1}{\partial z}-v_1\theta\frac{\partial(1-s_m)c_3}{\partial z}-\mu_l\theta c_1-\rho_b\mu_s s_1 \quad (1)$$

where, $c_1\left[\frac{M}{L^3}\right]$ is the mass concentration of colloid 1 in aqueous phase (mass of colloid 1 per unit volume of aqueous phase), $s_1\left[\frac{M}{M}\right]$ is the concentration of colloid 1 attached to grain surface (mass of colloid 1 per unit mass of dry soil), $s_m\left[\frac{M}{M}\right]$ is the mass fraction of colloid 2 in heteroaggregates in the aqueous phase (mass of colloid 2 per unit mass of heteroaggregates in aqueous phase), $c_3\left[\frac{M}{L^3}\right]$ is the mass concentration of heteroaggregates in the aqueous phase (mass of heteroaggregates per unit volume of aqueous phase), $s_{im}\left[\frac{M}{M}\right]$ is the mass fraction of colloid 2 in heteroaggregates at the grain surface (mass of colloid 2 per unit mass of heteroaggregates at grain surface), $s_3\left[\frac{M}{M}\right]$ is the mass concentration of heteroaggregates adsorbed at the grain surface (mass of heteroaggregates per unit mass of dry soil), θ [−] is the porosity of the soil, $\rho_b\left[\frac{M}{L^3}\right]$ is the bulk density of soil, ${D_L}^1\left[\frac{L^2}{T}\right]$ is the dispersion coefficient of colloid 1, $v_1\left[\frac{L}{T}\right]$ is the pore-water velocity of colloid 1, $\mu_l\left[\frac{1}{T}\right]$ is the inactivation rate coefficient of colloid 1 in the aqueous phase, and $\mu_s\left[\frac{1}{T}\right]$ is the inactivation rate coefficient of colloid 1 at the grain surface.

The deposition of colloid 1 on the grain surface is described either using a one-site reversible kinetic model or a two-site kinetic model with site 1 being reversible and site 2 being irreversible.

For one-site kinetic model, the governing equation is

$$\rho_b\frac{\partial s_1}{\partial t}=k_{1cs}c_1\theta-k_{1sc}\rho_b s_1-\rho_b\mu_s s_1 \quad (2)$$

For two-site kinetic model, the governing equations are

$$\rho_b\frac{\partial s_{11}}{\partial t}=k_{11cs}c_1\theta-k_{11sc}\rho_b s_{11}-\rho_b\mu_s s_{11} \quad (3a)$$

$$\rho_b\frac{\partial s_{12}}{\partial t}=k_{12cs}c_1\theta-\rho_b\mu_s s_{12} \quad (3b)$$

$$s_1=s_{11}+s_{12} \quad (3c)$$

where, $k_{1cs}\left[\frac{1}{T}\right]$ and $k_{1sc}\left[\frac{1}{T}\right]$ are the rate coefficients for attachment and detachment of colloid 1 at grain surface for a one-site kinetic model, respectively, $s_{11}\left[\frac{M}{M}\right]$ and $s_{12}\left[\frac{M}{M}\right]$ represent the concentration of colloid 1 attached to site 1 and site 2, respectively, for a two-site kinetic model, and $k_{11cs}\left[\frac{1}{T}\right]$, $k_{11sc}\left[\frac{1}{T}\right]$, and $k_{12cs}\left[\frac{1}{T}\right]$ represent rate coefficients for attachment of colloid 1 to site 1, detachment of colloid 1 from site 1, and attachment of colloid 1 to site 2 for a two-site kinetic model, respectively.

The transport equation for colloid 2 can be written as

$$\theta\frac{\partial c_2}{\partial t}+\rho_b\frac{\partial s_2}{\partial t}+\theta\frac{\partial(s_m c_3)}{\partial t}+\rho_b\frac{\partial(s_{im}s_3)}{\partial t}=\theta {D_L}^2\frac{\partial^2 c_2}{\partial z^2}+\theta {D_L}^1\frac{\partial^2(s_m c_3)}{\partial z^2} - v_2\theta\frac{\partial c_2}{\partial z}-v_1\theta\frac{\partial(s_m c_3)}{\partial z} \quad (4)$$

where, $c_2\left[\frac{M}{L^3}\right]$ is the mass concentration of colloid 2 in aqueous phase (mass of colloid 2 per unit volume of aqueous phase), and $s_2\left[\frac{M}{M}\right]$ is the concentration of colloid 2 attached to grain surface (mass of colloid 2 per unit mass of dry soil), ${D_L}^2\left[\frac{L^2}{T}\right]$ is the dispersion coefficient of colloid 2, and $v_2\left[\frac{L}{T}\right]$ is the pore-water velocity of colloid 2.

The governing equation for the deposition of colloid 2 on grain surface is described using either a one-site reversible kinetic model without/with blocking or a two-site kinetic model with site 1 being reversible and site 2 being irreversible.

For one-site kinetic model without blocking, the governing equation is

$$\rho_b\frac{\partial s_2}{\partial t}=k_{2cs}c_2\theta-k_{2sc}\rho_b s_2 \quad (5)$$

For one-site kinetic model with blocking, the governing equation is

$$\rho_b\frac{\partial s_2}{\partial t}=k_{2cs}\left(1-\frac{s_2}{s_{2max}}\right)c_2\theta-k_{2sc}\rho_b s_2 \quad (6)$$

For two-site kinetic model, the governing equations are

$$\rho_b\frac{\partial s_{21}}{\partial t}=k_{21cs}c_2\theta-k_{21sc}\rho_b s_{21} \quad (7a)$$

$$\rho_b\frac{\partial s_{22}}{\partial t}=k_{22cs}c_2\theta \quad (7b)$$

$$s_2=s_{21}+s_{22} \quad (7c)$$

where, $k_{2cs}\left[\frac{1}{T}\right]$ and $k_{2sc}\left[\frac{1}{T}\right]$ are the rate coefficients for attachment and detachment of colloid 2 at grain surface for a one-site kinetic model, respectively, $s_{2max}\left[\frac{M}{M}\right]$ is the maximum adsorption capacity of the grain surface for colloid 2, $s_{21}\left[\frac{M}{M}\right]$ and $s_{22}\left[\frac{M}{M}\right]$ represent the concentration of colloid 2 attached to site 1 and site 2, respectively, and $k_{21cs}\left[\frac{1}{T}\right]$, $k_{21sc}\left[\frac{1}{T}\right]$ and $k_{22cs}\left[\frac{1}{T}\right]$ represent rate coefficients for attachment of colloid 2 to site 1, detachment of colloid 2 from site 1, and attachment of colloid 2 to site 2 for a two-site kinetic model, respectively.

The governing equation for the transport of heteroaggregates in aqueous phase is given by

$$\theta\frac{\partial c_3}{\partial t}=\theta {D_L}^1\frac{\partial^2 c_3}{\partial z}-v_1\theta\frac{\partial c_3}{\partial z}+k_a c_1\theta+k_a c_2\theta-k_d c_3\theta-k_{a(agg)}c_3\theta+k_{d(agg)}s_3\rho_b - \mu_l\theta(1-s_m)c_3 \quad (8)$$

where, $k_a\left[\frac{1}{T}\right]$ represents the rate coefficient for attachment of colloid 1 to colloid 2 and vice versa, $k_d\left[\frac{1}{T}\right]$ represents the rate coefficient for

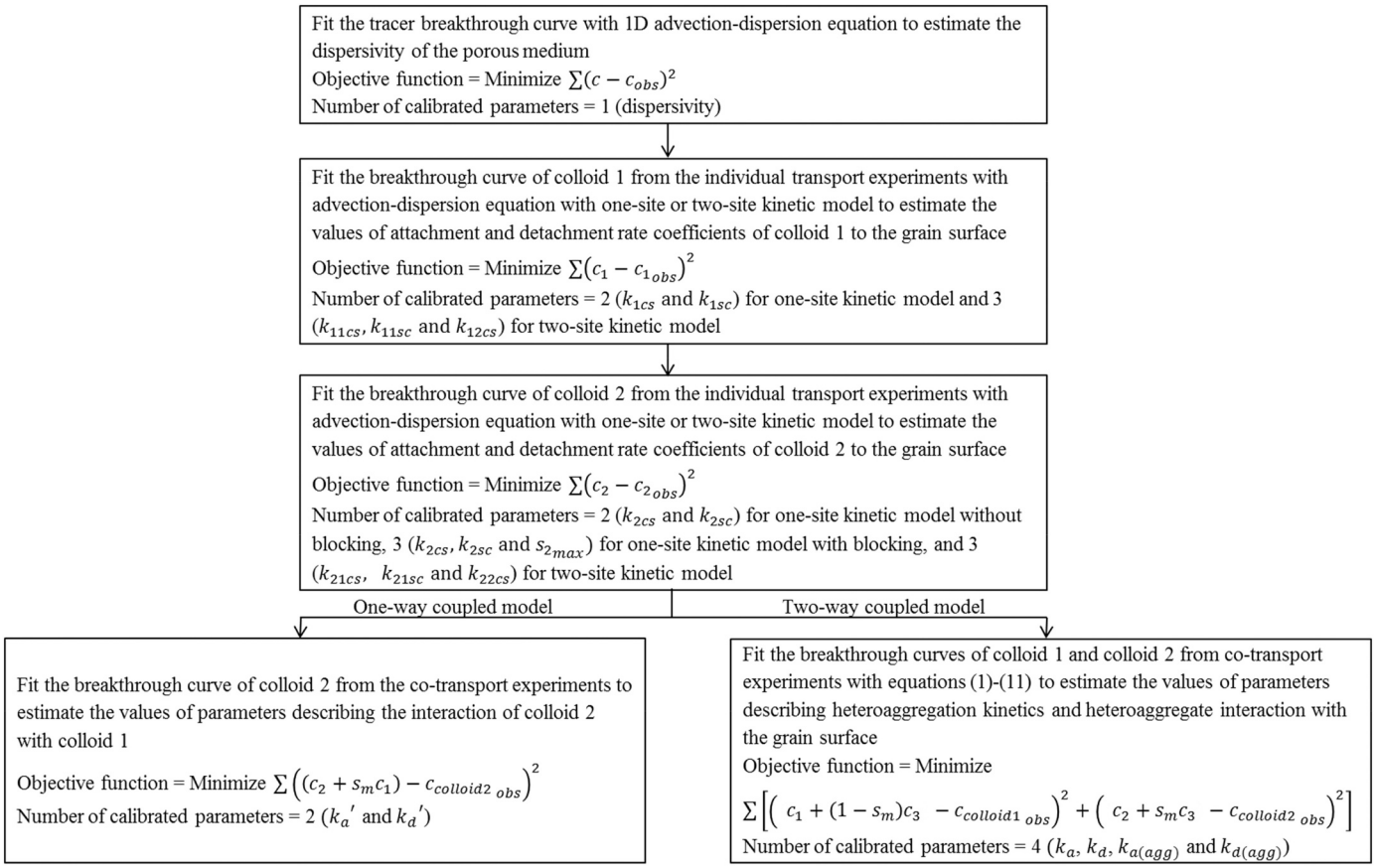

Fig. 2. Fitting procedure for one-way and two-way coupled models. c and c_{obs} represent the model fitted and the experimentally measured concentration of tracer, c_{1obs} and c_{2obs} are the experimentally measured concentration of colloid 1 and colloid 2 from individual transport experiments. $c_{colloid1obs}$ and $c_{colloid2obs}$ are the experimentally measured total mobile concentration of colloid 1 and colloid 2 from co-transport experiments.

detachment of colloid 1 from colloid 2 and vice versa, $k_{a(agg)}$ $\left[\frac{1}{T}\right]$ represents the rate coefficient for attachment of heteroaggregates to grain surface, and $k_{d(agg)}$ $\left[\frac{1}{T}\right]$ represents the rate coefficient for detachment of heteroaggregates from grain surface.

The deposition of the heteroaggregates to the grain surface is given by

$$\rho_b \frac{\partial s_3}{\partial t} = k_a c_1 \theta + k_a c_2 \theta - k_d \rho_b s_3 + k_{a(agg)} c_3 \theta - k_{d(agg)} s_3 \rho_b - \mu_s \rho_b (1 - s_{im}) s_3 \tag{9}$$

The mass balance for colloid 2 in heteroaggregates in aqueous phase is given by.

$$\theta \frac{\partial (s_m c_3)}{\partial t} = \theta D_L{}^1 \frac{\partial^2 (s_m c_3)}{\partial z} - v_1 \theta \frac{\partial (s_m c_3)}{\partial z} + k_a c_2 \theta - k_d \theta (s_m c_3) - k_{a(agg)} \theta (s_m c_3) + k_{d(agg)} \rho_b (s_{im} s_3) \tag{10}$$

The mass balance for colloid 2 in heteroaggregates adsorbed to the grain surface is given by

$$\rho_b \frac{\partial (s_{im} s_3)}{\partial t} = k_a c_2 \theta - k_d \rho_b (s_{im} s_3) + k_{a(agg)} \theta (s_m c_3) - k_{d(agg)} \rho_b (s_{im} s_3) \tag{11}$$

2.2. Solution of the governing equations

Eqs. (1), (2), (4), (5), (8)–(11) describe the governing equations of the two-way coupled model for the co-transport of two different colloids in porous media with both colloids undergoing one-site linear kinetic sorption at the grain surface without blocking. They comprise eight equations for eight unknowns (c_1,s_1, c_2, s_2, c_3, s_3, s_m, s_{im}). When colloid 2 undergoes blocking, Eq. (5) must be replaced with Eq. (6). When both colloids undergo two-site linear kinetic sorption at the grain surface, then Eqs. (1), (3), (4), (7)–(11) represent the complete set of ten equations for ten unknowns (c_1, s_{11}, s_{12}, c_2, s_{21}, s_{22}, c_3, s_3, s_m, s_{im}). The initial concentrations of colloid 1 and colloid 2 in all forms in the porous medium are assumed to be zero. The complete set of governing Eqs. (1)–(11) is solved by applying the following set of boundary conditions.

$$c_1(0,t) = \begin{cases} c_{10}, t \le t_{in} \\ 0, t > t_{in} \end{cases} \tag{12}$$

$$c_2(0,t) = \begin{cases} c_{20}, t \le t_{in} \\ 0, t > t_{in} \end{cases} \tag{13}$$

$$c_3(0,t) = s_m(0,t) = 0 \tag{14}$$

$$\left.\frac{\partial c_1}{\partial z}\right|_{(L,t)} = \left.\frac{\partial c_2}{\partial z}\right|_{(L,t)} = \left.\frac{\partial c_3}{\partial z}\right|_{(L,t)} = \left.\frac{\partial (s_m)}{\partial z}\right|_{(L,t)} = 0 \tag{15}$$

where, c_{10} and c_{20} are the inlet concentrations for the free forms of colloid 1 and colloid 2, respectively, t_{in} is the duration of input pulse for colloid 1 and colloid 2, and L is the length of the porous medium domain. Eqs. (12)–(13) indicate a Dirichlet boundary condition for the free form of colloids 1 and 2 at inlet. Eq. (14) indicates a zero inlet concentration for the heteroaggregates in aqueous phase. Eq. (15) indicates a Neumann type boundary condition at the outlet for the mobile forms of colloids 1 and 2.

The governing Eqs. (1), (2) (or (3)), (4), (5) (or (6) or (7)), (8), (9), (10), and (11) subject to the initial and boundary conditions are solved

numerically using an alternating three-step operator splitting approach (Seetha et al., 2015). This numerical scheme involves splitting the governing equations into advection, dispersion and reaction operators and then solving them sequentially for the first half of every time step. The order of solution is then reversed in the second half of every time step. The advection, dispersion and reaction operators are solved using an explicit finite volume scheme with minmod limiter, implicit finite difference method and fourth-order Runge-Kutta method, respectively. More details about the above numerical scheme are given in Seetha et al. (2015).

3. One-way coupled model

The one-way coupled model has been the most common approach to simulate the co-transport of two different colloids in porous media. This model assumes that the transport properties of colloid 1 are not affected by the presence of colloid 2 on its surface, and does not account for heteroaggregation kinetics. Though this model is already available in the literature (Seetha et al., 2015; Vasiliadou and Chrysikopoulos, 2011), the governing equations are reproduced in the appendix (Eqs. (A1) to (A5)) to maintain the consistency in the notations throughout this paper.

4. Model evaluation

The developed two-way coupled model is evaluated by reproducing the observed behaviour in several sets of experiments reported in four publications (Chrysikopoulos et al., 2017; Georgopoulou et al., 2020; Syngouna and Chrysikopoulos, 2013; Syngouna et al., 2017). These experiments involved studying the co-transport of a micrometer-sized colloid (kaolinite, montmorillonite, *Escherichia coli*(*E. coli*), *Enterococcus faecalis*(*E. faecalis*), or *Staphylococcus aureus*(*S. aureus*)) and a nanometer-sized colloid (graphene oxide (GO) nanoparticles, MS2, φx174, or adenovirus). The general scheme of all column experiments was as follows: First, the dispersivity of the porous medium was determined by performing a tracer experiment. Then, the transport of each colloid (large or small) was studied in separate experiments to understand their individual deposition behaviour onto the grain surface. This was followed by co-transport experiments involving simultaneous injection of both the micrometer- and nanometer-sized colloids into the column.

4.1. Description of fitting procedure

The procedure for fitting the experimental data with the one-way and two-way coupled models along with the objective function and the number of calibrated parameters in each step is given in the form of a flow chart in Fig. 2. For fitting the experimental data, first, the value of dispersivity of the porous medium is estimated by fitting the tracer breakthrough curve with 1D advection-dispersion equation. It is known that colloid dispersivity is size dependent and can be different from tracer dispersivity (Chrysikopoulos and Katzourakis, 2015; Keller et al., 2004). Nevertheless, except in the case of Georgopoulou et al. (2020), we assume colloids dispersivity to be the same as the tracer dispersivity, in order to reduce the number of fitted parameters,. Also, all colloids are assumed to travel at the same velocity as the pore water. Ofcourse, the correct procedure would have been to estimate the values of velocity and dispersivity along with the deposition parameters for each colloid by fitting colloid breakthrough curve with advection-dispersion-sorption equation. However, we find that the available experimental data do not contain sufficient information to warrant estimating so many parameters independently. The aforementioned procedure for estimating dispersivity was the same for both one-way and two-way models. Next, for the one-way coupled model, breakthrough curves of colloid 1 and colloid 2 from the individual transport experiments are fitted with advection-dispersion equation with one-site or two-site kinetic model to estimate the values of attachment and detachment rate coefficients for colloid 1 to the grain surface (k_{1cs} and k_{1sc} or k_{11cs}, k_{11sc} and k_{12cs}) and for colloid 2 (k_{2cs} *and* k_{2sc} or k_{2cs}, k_{2sc} and s_{2max} or k_{21cs}, k_{21sc} and k_{22cs}). The governing equations for the individual transport of colloid 1 and colloid 2 are given in Appendix B. In line with the underlying assumption of one-way coupled model, parameter values for individual particles of both colloid 1 and colloid 2, either in aqueous phase or adsorbed, are assumed to remain unchanged when simulating co-transport experiments. Then, the breakthrough curve of colloid 2 from the co-transport experiments is fitted to estimate the values of parameters describing the interaction of colloid 2 with colloid 1 ($k_a^{'}$ and $k_d^{'}$, where $k_a^{'}$ and $k_d^{'}$ are the rate coefficients for attachment and detachment of colloid 2 to colloid 1). In all four papers used for model evaluation, the effluent breakthrough curves were reported in terms of the total mobile concentration of colloid 1 and colloid 2 (Chrysikopoulos et al., 2017; Georgopoulou et al., 2020; Syngouna and Chrysikopoulos, 2013; Syngouna et al., 2017). In the one-way coupled model, this would correspond to c_1 and $(c_2 + s_m c_1)$, respectively. In addition, Syngouna and Chrysikopoulos (2013) also reported the breakthrough concentration of colloid 2 alone in the free form (c_2).

Next, we explain the step-by-step procedure for fitting the experimental data for the co-transport of two different colloids with the two-way coupled model. The estimation of dispersivity of porous medium, and the attachment and detachment rate coefficients of colloid 1 and colloid 2 to the grain surface are the same as explained in the previous paragraph. After knowing the values of individual deposition parameters of colloid 1 and colloid 2, breakthrough curves of colloid 1 and colloid 2 from the co-transport experiments are fitted with Eqs. (1)–(11) to estimate the values of parameters describing heteroaggregation kinetics (k_a and k_d) and heteroaggregate interaction with the grain surface ($k_{a(agg)}$ and $k_{d(agg)}$). In our model, the total mobile concentrations of colloid 1 and colloid 2 would correspond to $(c_1 + (1 - s_m)c_3)$ and $(c_2 + s_m c_3)$, respectively, and the free form of colloid 2 would correspond to c_2. We used Levenberg-Marquardt algorithm to find the best fit between the observed and the modelled breakthrough curves for colloid 1 and colloid 2.

The performance of the one-way and two-way coupled models is compared quantitatively using information theoretic criteria *AIC* and *AICc*, and Bayesian criteria (*BIC*), which serve as model selection criteria (Ye et al., 2008). These criteria favour the model which reproduces the experimental data closely and having the least number of fitting parameters. The model with the lowest value of a given criterion is the preferred model. *AIC*, *AICc* and *BIC*are calculated as (Ye et al., 2008):

$$AIC = n_{obs} ln\left(\sigma^2\right) + 2P \tag{16}$$

$$AICc = n_{obs} ln\left(\sigma^2\right) + 2P + \frac{2N(N+1)}{n_{obs} - N - 1} \tag{17}$$

$$BIC = n_{obs} ln\left(\sigma^2\right) + P\, ln(n_{obs}) \tag{18}$$

where n_{obs} is the number of observations, σ^2 is the sum of squared residuals divided by the number of observations, P is the number of model parameters estimated, and $N = P + 1$.

4.2. Simulating experimental results of Chrysikopoulos et al. (2017)

Chrysikopoulos et al. (2017) conducted laboratory column experiments to study the influence of pH and ionic strength on the co-transport of GO nanoparticles and kaolinite colloids under saturated conditions. Obviously, in our model, kaolinite is colloid 1 and GO nanoparticles are colloid 2. Two types of porous media were used in this study: glass beads and quartz sand. The column was 30 cm long with a diameter of 2.5 cm. The porosity and bulk density of glass beads were 0.42 and 1.68 g/cm^3, respectively. The respective values for quartz sand were 0.39 and 1.7 g/cm^3. The hydrodynamic diameters of GO nanoparticles and kaolinite

Table 1
Fitted parameters using two-way and one-way coupled models for the experimental results of Chrysikopoulos et al. (2017)[a]

Porous medium			Glass beads					Quartz sand
pH			4	7	10	7	7	7
IS			7	7	7	12	27	7
Tracer		Dispersivity (cm)	0.136					0.380
Individual transport	Kaolinite	k_{11cs}(/min)	0.016 (0.003)	0.030 (0.002)	0.028 (0.003)	0.040 (0.003)	0.038 (0.005)	2.531 (2.83×10^5)
		k_{11sc}(/min)	0.172 (0.038)	0.159 (0.014)	0.179 (0.025)	0.215 (0.018)	0.309 (0.042)	13.428 (1.5×10^6)
		k_{12cs}(/min)	0.019 (0.0002)	0.008 (0.0001)	0.007 (0.0002)	0.009 (0.0001)	0.015 (0.0001)	0.009 (0.093)
		R^2	0.99	0.99	0.99	0.99	0.99	0.99
	GO nanoparticles	k_{21cs}(/min)	0.035 (0.006)	0.020 (0.003)	0.029 (0.005)	0.022 (0.002)	0.023 (0.003)	2.536 (6.41×10^5)
		k_{21sc}(/min)	0.133 (0.031)	0.177 (0.031)	0.214 (0.043)	0.179 (0.023)	0.166 (0.026)	13.424 (3.39×10^6)
		k_{22cs}(/min)	0.002 (0.0005)	0.001 (0.0002)	0.000 (0.0002)	0.001 (0.0002)	0.002 (0.0002)	0.004 (0.037)
		R^2	0.98	0.99	0.99	0.99	0.99	0.95
Co-transport (two-way coupled model)		k_a(/min)	0.123 (0.048)	0.101 (0.017)	0.106 (0.041)	0.109 (0.013)	0.110 (0.016)	0.134 (0.024)
		k_d(/min)	1.446 (2.790)	1.309 (1.72)	2.781 (76.89)	7.016 (39.176)	19.820 (245.881)	1.158 (0.839)
		$k_{a(agg)}$(/min)	26.114 (200.43)	25.033 (1046.98)	21.486 (2202.55)	19.830 (693.47)	7.751 (136.619)	25.394 (477.510)
		$k_{d(agg)}$(/min)	0	0	0	0	0	0
		R^2(kaolinte)	0.74	0.85	0.88	0.72	0.95	0.95
		R^2(GO nanoparticles)	NA	0.96	0.95	0.97	0.86	0.67
		AIC	−365.49	−659.88	−636.95	−680.36	−550.44	−479.85
		AICc	−364.75	−659.15	−636.20	−679.60	−549.68	−479.12
		BIC	−359.26	−653.60	−630.77	−674.18	−544.25	−473.56
Co-transport (one-way coupled model)		k_a'(/min)	0.016 (0.003)	0.033 (0.019)	0.002 (0.0003)	0.002 (0.0003)	0.004 (0.0003)	0.026 (0.014)
		k_d'(/min)	0.002 (0.001)	0.317 (0.219)	0.000 (0.001)	0.000	0.000	0.008 (0.003)
		R^2(GO nanoparticles)	0.87	0.96	0.99	0.99	0.97	0.81
		AIC	−286.26	−295.65	−372.35	−370.58	−374.35	−231.80
		AICc	−285.33	−294.73	−371.39	−370.12	−373.89	−230.88
		BIC	−283.45	−292.85	−369.61	−369.21	−372.98	−229.00
Co-transport (one-way coupled model): Simulating the kaolinite breakthrough curve		R^2(kaolinte)	NA	NA	NA	NA	NA	NA

NA: Not applicable as the fitting is poor.
[a] The standard errors associated with the estimated parameter values are given in parentheses.

were in the range of 413–654 nm, and 513–709 nm, respectively. Experiments were conducted at a flow rate of 1.5 mL/min and at three different values of pH (4, 7, 10) and ionic strength (7, 12, 27 mM). The inlet concentrations of kaolinite and GO nanoparticles were 50 mg/L and 5 mg/L, respectively. Each experiment consisted of injecting appropriate colloidal suspensions (kaolinite or GO nanoparticles or simultaneous injection of kaolinite and GO nanoparticles) for 3 pore volumes (PVs), followed by flushing the column with colloid-free background solution for 2 PVs. All experiments were conducted at room temperature. More details about the experiments are given in Chrysikopoulos et al. (2017).

Chrysikopoulos et al. (2017) observed greater retention and larger collision efficiency of both GO nanoparticles and kaolinite during their co-transport than during their individual transport. The deposition of kaolinite and GO nanoparticles to the grain surface is described using a two-site kinetic model (Appendix B). The estimated values of the various parameters for the two-way and one-way coupled models are given in Table 1. Fig. 3 compares the observed and fitted breakthrough curves of kaolinite and GO nanoparticles during their co-transport through columns packed with glass beads at various pH and ionic strength values of the background solution. The simulated breakthrough curves from the two-way coupled model matches the observed data reasonably well for all cases, except for the breakthrough curve of GO nanoparticles at pH = 4 and ionic strength =7 mM through glass bead packed columns (Fig. 3b). Fig. 4 compares the observed and fitted breakthrough curves of kaolinite and GO nanoparticles during their co-transport through columns packed with quartz sand at pH = 7 and ionic strength =7 mM. The one-way coupled model could not simulate the observed breakthrough curves of kaolinite for any of the co-transport experiments (Figs. 3 and 4, and Table 1). The values of *AIC*, *AICc*, and *BIC* for the two-way coupled model are smaller than the one-way coupled model, which indicates that the latter is the most preferred model. Chrysikopoulos et al. (2017) observed from the co-transport experimental data that GO nanoparticle retention inside porous medium increased with decreasing pH due to the possible increase in heteroaggregation. This is supported by the experimental results of Sotirelis and Chrysikopoulos (2017) who observed from batch experiments a greater attachment of GO particles onto kaolinite colloids with decreasing pH. This is due to less negative surface potential of kaolinite colloids and GO nanoparticles with decreasing pH, which leads to greater attraction between them as a result of deeper secondary minimum. This agrees with the estimated parameters for the two-way coupled model given in Table 1, which shows that the ratio of attachment and detachment rate coefficients of GO nanoparticles to kaolinite colloids increases with decreasing pH. Further, Table 1 shows that the attachment rate coefficient of heteroaggregates to the grain surface increases with decreasing pH. Since the surface potentials of both GO nanoparticles and kaolinite become less negative with decreasing pH, the surface potential of heteroaggregates may also decrease, resulting in more attachment to the grain surfaces. Also, Table 1 indicates that the attachment of GO nanoparticles to kaolinite increased slightly with increasing ionic strength. This is in line with the observations of Sotirelis and Chrysikopoulos (2017) who found from batch experiments that the mass of GO nanoparticles attached to kaolinite colloids increased with ionic strength due to less negative zeta

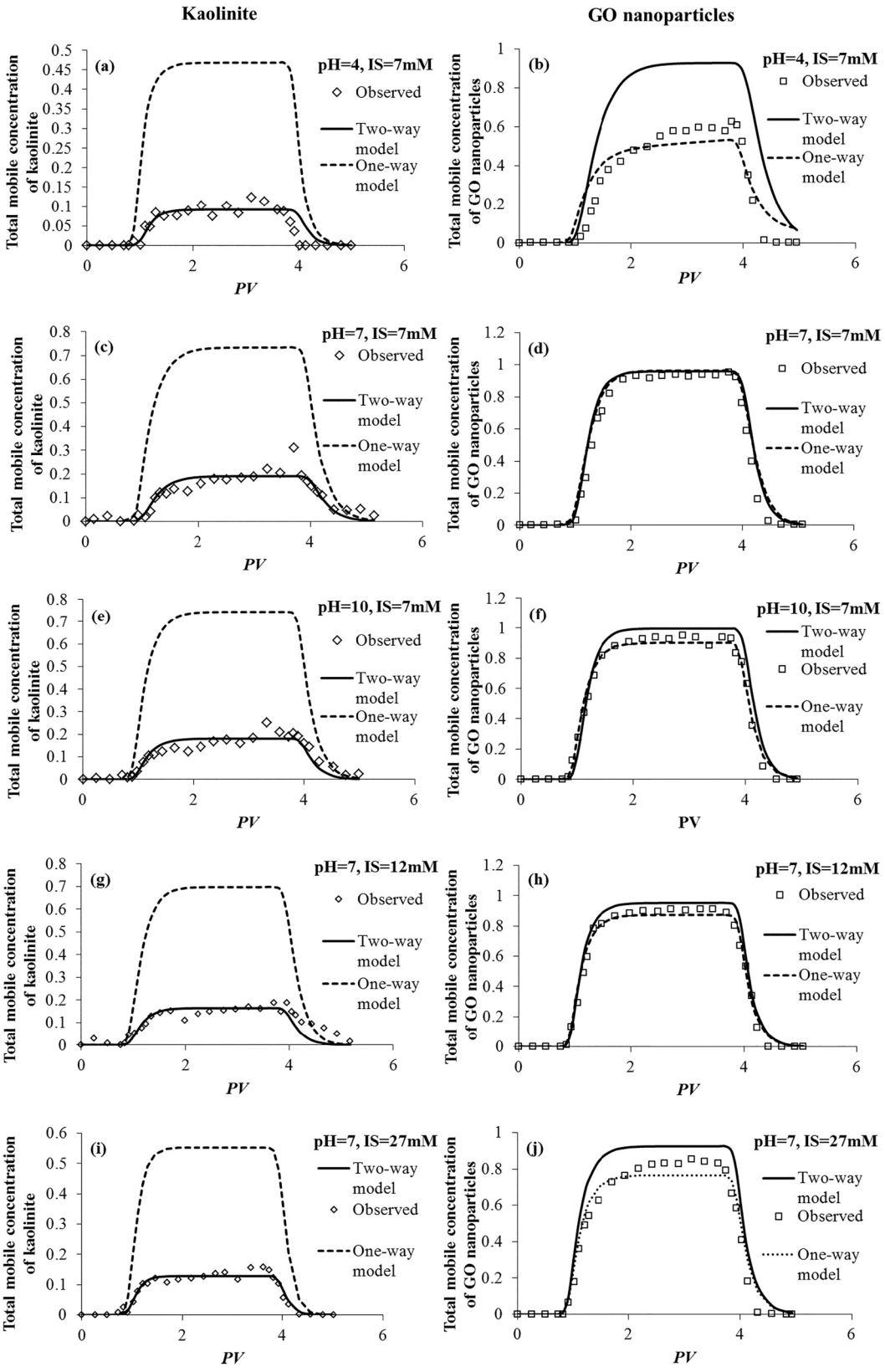

Fig. 3. Observed and fitted breakthrough curves for the co-transport of kaolinite and GO nanoparticles through glass bead packed column (experiments of Chrysikopoulos et al., 2017): total mobile concentrations of kaolinite (a, c, e, g, i) and GO (b, d, f, h, j) at (a, b) pH = 4, ionic strength = 7 mM, (c, d) pH = 7, ionic strength = 7 mM, (e, f) pH = 10, ionic strength = 7 mM, (g, h) pH = 7, ionic strength = 12 mM, and (i, j) pH = 7, ionic strength = 27 mM.

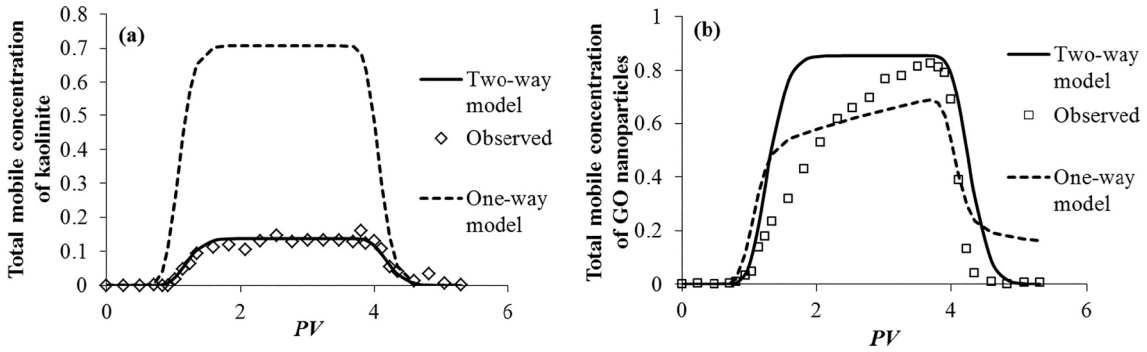

Fig. 4. Observed and fitted breakthrough curves for the co-transport of kaolinite and GO nanoparticles through quartz sand packed column (experiments of Chrysikopoulos et al., 2017): total mobile concentrations of kaolinite (a) and GO (b) at pH = 7 and ionic strength = 7 mM.

Table 2
Fitted parameters using two-way and one-way coupled models for the experimental results of Syngouna et al. (2017)[a]

Clay colloid			Kaolinite			Montmorillonite		
Flow rate (mL/min)			2.5	1.5	0.8	2.5	1.5	0.8
Tracer		Dispersivity (cm)	0.072	0.136	0.180	0.072	0.136	0.180
Individual transport	Clay colloid	k_{11cs} (/min)	0.192 (0.069)	0.049 (0.012)	0.019 (0.004)	0.124 (0.019)	0.029 (0.004)	0.014 (0.002)
		k_{11sc} (/min)	0.233 (0.09)	0.114 (0.029)	0.018 (0.006)	0.121 (0.022)	0.025 (0.005)	0.020 (0.006)
		k_{12cs} (/min)	0.049 (0.002)	0.026 (0.0006)	0.016 (0.0008)	0.017 (0.001)	0.003 (0.001)	0.005 (0.0006)
		R^2	0.89	0.94	0.87	0.96	0.91	0.92
	Adenovirus	k_{21cs} (/min)	0.993 (1.000)	0.014 (0.008)	0.008 (0.002)	0.993 (1.000)	0.014 (0.008)	0.008 (0.002)
		k_{21sc} (/min)	1.884 (1.920)	0.051 (0.039)	0.027 (0.01)	1.884 (1.920)	0.051 (0.039)	0.027 (0.01)
		k_{22cs} (/min)	0.064 (0.002)	0.027 (0.001)	0.018 (0.0005)	0.064 (0.002)	0.027 (0.001)	0.018 (0.0005)
		R^2	0.89	0.89	0.95	0.89	0.89	0.95
Co-transport (two-way coupled model)		k_a (/min)	0.036 (0.006)	0.012 (0.002)	0.023 (0.004)	0.037 (0.004)	0.018 (0.005)	0.011 (0.002)
		k_d (/min)	6.62×10^{-5} (2.16×10^{-5})	0.000	0.000	0.000	0.000	0.000
		$k_{a(agg)}$ (/min)	0.077 (0.008)	0.066 (0.016)	0.026 (0.001)	0.076 (0.007)	0.169 (0.307)	0.042 (0.016)
		$k_{d(agg)}$ (/min)	2.09×10^{-4} (6.38×10^{-5})	5.28×10^{-6} (1.86×10^{-6})	1.17×10^{-5} (4.61×10^{-6})	0.000	0.000	0.000
		R^2 (clay)	0.89	0.97	0.95	0.64	0.74	0.75
		R^2(adenovirus)	0.51	0.96	0.88	0.75	NA	NA
		AIC	−837.97	−998.90	−903.06	−758.91	−717.87	−657.57
		AICc	−836.90	−998.15	−902.17	−758.50	−717.42	−657.04
		BIC	−829.46	−992.72	−897.33	−754.66	−713.75	−653.74
Co-transport (one-way coupled model)		k_a' (/min)	0.034 (0.038)	0.035 (0.044)	0.014 (0.013)	NA	0.005 (0.006)	NA
		k_d' (/min)	0.000	0.000	0.000	NA	0.000	NA
		R^2(adenovirus)	0.03	0.66	NA	NA	NA	NA
		AIC	−348.48	−361.36	−285.25	NA	−202.81	NA
		AICc	−348.05	−360.90	−284.70	NA	−202.35	NA
		BIC	−347.05	−360.00	−284.03	NA	−201.45	NA
Co-transport (one-way coupled model): Simulating the clay colloid breakthrough curve		R^2 (clay)	NA	NA	NA	NA	NA	NA

NA: Not applicable as the fitting is poor.
[a] The standard errors associated with the estimated parameter values are given in parentheses.

potentials of GO nanoparticles and kaolinite with increasing ionic strength and thus less repulsion between them. The attachment rate coefficient of heteroaggregates to the grain surface and GO nanoparticle attachment to kaolinite is found to be larger for sand than for glass beads (Table 1). This is in agreement with the observations of Chrysikopoulos et al. (2017) who found greater retention and larger collision efficiency of GO nanoparticles in columns packed with quartz sand than glass beads. Though the zeta potential of the sand and the energy profiles for GO nanoparticle-quartz sand and kaolinite-quartz sand are similar to those in the presence of glass beads (Chrysikopoulos et al., 2017), the greater retention of GO nanoparticles on sand may be due to the heterogeneity of the sand surface as compared to the glass beads.

4.3. Simulating experimental results of Syngouna et al. (2017)

Syngouna et al. (2017) conducted experiments to study the co-transport of clay colloids (kaolinite and montmorillonite) and human adenovirus through laboratory columns. In our model, they are colloid 1 and colloid 2, respectively. Columns of 2.5 cm in diameter and 30 cm in length were packed with glass beads under saturated conditions. The dry bulk density of the porous medium was 2.65 g/cm^3 and porosity was 0.42. Sterile Dnase-I reaction solution was used as the background

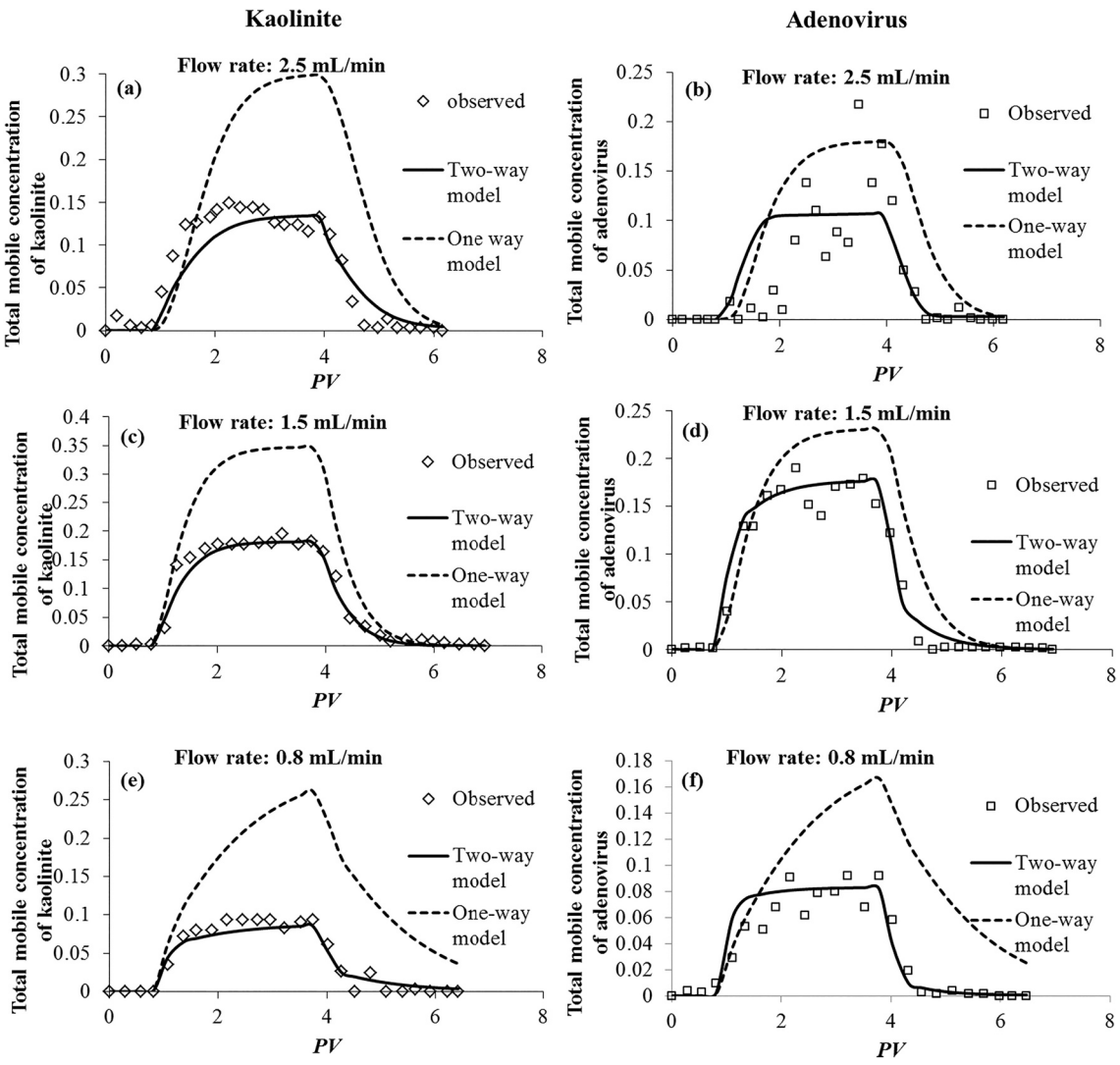

Fig. 5. Observed and fitted breakthrough curves for the co-transport of kaolinite and adenovirus (experiments of Syngouna et al., 2017): total mobile concentrations of kaolinite (a, c, e) and adenovirus (b, d, f) at flow rates of 2.5 mL/min (a and b), 1.5 mL/min (c and d), and 0.8 mL/min (e and f).

solution. The size of kaolinite particles was in the range of 0.2–1 μm and the average size of montmorillonite particles was 0.5 μm. Adenovirus size is in the range of 65–85 nm. Two sets of experiments were performed in this study. The first set of experiments involved studying the individual transport behaviour of kaolinite, montmorillonite and adenovirus, and the second set involved studying the co-transport behaviour of clay colloids and adenovirus. Each co-transport experiment involved passing clay and adenovirus suspension simultaneously for 3 PVs through the column, followed by flushing the column with 3PVs of colloid-free background solution. A total of six experiments were reported in this study for the co-transport of kaolinite-adenovirus and montmorillonite-adenovirus at three different flow rates of 0.8, 1.5 and 2.5 mL/min. The effluent total suspended virus concentration and the effluent total clay concentration were measured using qPCR and UV-VIS spectrophotometer, respectively. More details about the experimental protocol are available in Syngouna et al. (2017). The influent concentrations of kaolinite, montmorillonite and adenovirus for the various experiments are given in Table 1 of Syngouna et al. (2017).

Syngouna et al. (2017) observed higher retention of both adenovirus and clay colloids when they were co-present than during their individual transport due to the formation of large clay-virus heteroaggregates that clogged the pores and the attachment of heteroaggregates to the grain surface. The interactions of kaolinite, montmorillonite and adenovirus with the grain surface are described using a two-site kinetic model (Appendix B). The inactivation of adenovirus is neglected in our model. Table 2 gives the fitted values of parameters for the two-way and one-way coupled models. The dispersivity values estimated by Seetha et al. (2015) by fitting the tracer breakthrough curves of Syngouna and Chrysikopoulos (2013) are used in this study. Figs. 5 and 6 show the comparisons of observed and the fitted breakthrough curves for the co-transport of kaolinite and adenovirus, and montmorillonite and adenovirus, respectively, at different flow rates. It is clear from Fig. 5 that the two-way coupled model could simulate the observed breakthrough curves for the co-transport of kaolinite and adenovirus reasonably well and the performance of the one-way coupled model is rather poor at all the flow rates. The values of *AIC*, *AICc*and *BIC* also indicate that two-way coupled model is preferable over the one-way coupled model (Table 2). Syngouna et al. (2017) found that the collision efficiency (attachment rate coefficient is proportional to collision efficiency) of clays and viruses was higher during co-transport experiments than during their individual transport. This is supported by the values of fitted parameters in Table 2 for a two-way coupled model which indicates that the kinetics of heteroaggregation and heteroaggregate deposition to the grain surface is irreversible (detachment rate coefficient is zero), whereas the deposition of clays and viruses to the grain surface is reversible during their individual transport. Syngouna et al. (2017) also observed that the values of

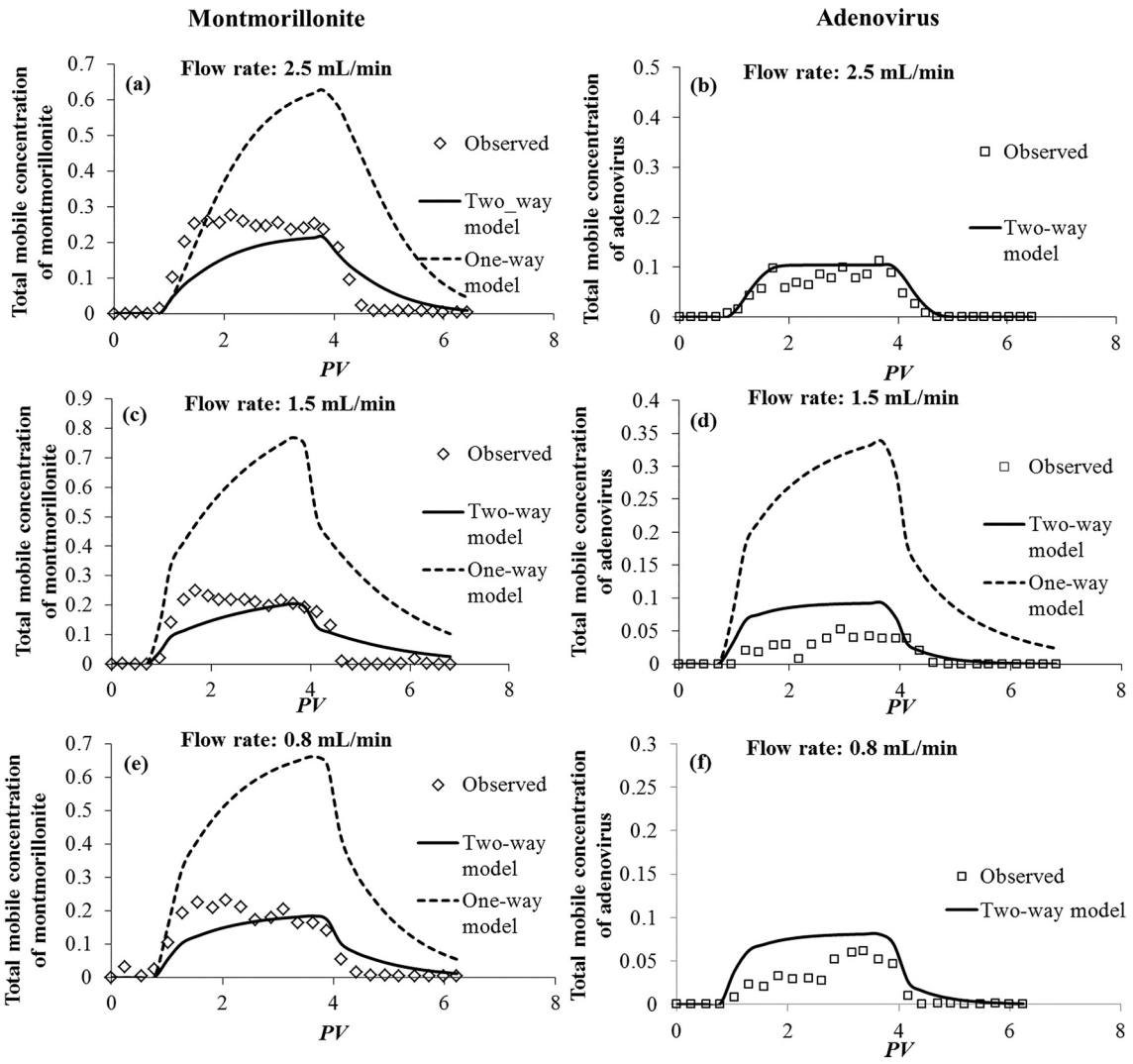

Fig. 6. Observed and fitted breakthrough curves for the co-transport of montmorillonite and adenovirus (experiments of Syngouna et al., 2017): total mobile concentrations of montmorillnite (a, c, e) and adenovirus (b, d, f) at flow rates of 2.5 mL/min (a and b), 1.5 mL/min (c and d), and 0.8 mL/min (e and f).

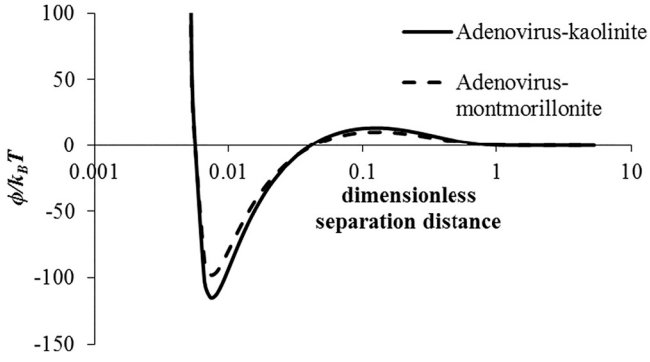

Fig. 7. DLVO energy profile between adenovirus and clay colloid.

collision efficiency increased with increasing flow rate during the co-transport studies. This is in line with the estimated values of parameters obtained in this study using a two-way coupled model for the co-transport of kaolinite and adenovirus: we have found that the rate coefficient of attachment of heteroaggregates to the grain surface increased with increasing flow rate (Table 2). This indicates that the kinetics of interaction of heteroaggregates with the grain surface controls kaolinite-adenovirus co-transport. Graphs shown in Fig. 6 and R^2-values given in Table 2 indicate that neither the two-way coupled model nor the one-way coupled model could satisfactorily fit the co-transport data of montmorillonite and adenovirus at all flow rates, except for the two-way coupled model at 2.5 mL/min. Further, Syngouna et al. (2017) observed greater retention of adenovirus in the presence of montmorillonite than kaolinite. The fitted values of k_a and k_a

Table 3
Fitted parameters using two-way and one-way coupled models for the experimental results of Syngouna and Chrysikopoulos (2013)[a].

Clay colloid		Kaolinite			Montmorillonite			Kaolinite			Montmorillonite		
Virus type		MS2			MS2			φx174			φx174		
Flow rate (mL/min)		0.8	1.5	2.5	0.8	1.5	2.5	0.8	1.5	2.5	0.8	1.5	2.5
Dispersivity (cm)		0.180	0.136	0.072	0.180	0.136	0.072	0.180	0.136	0.072	0.180	0.136	0.072
Co-transport (two-way coupled model)	k_a (/min)	0.030 (0.007)	0.034 (0.009)	0.036 (0.004)	0.003 (5.5×10^{-4})	0.015 (0.001)	0.030 (0.003)	0.004 (3.76×10^{-4})	0.016 (0.002)	0.018 (0.002)	0.005 (3.05×10^{-4})	0.011 (0.001)	0.017 (0.001)
	k_d (/min)	0.068 (0.012)	0.000	0.000	0.002 (6.61×10^{-4})	0.001 (5.76×10^{-4})	0.000	0.000	0.001 (6.9×10^{-4})	0.000	0.000	7.8×10^{-4} (0.001)	0.000
	$k_{a(agg)}$ (/min)	0.548 (2.081)	1.59×10^{-4} (1.07×10^{-4})	0.005 (0.003)	4.530 (202.731)	0.004 (0.001)	0.037 (0.006)	0.029 (0.015)	0.026 (0.006)	0.127 (0.105)	0.033 (0.009)	5.052 (148.49)	0.033 (0.008)
	$k_{d(agg)}$ (/min)	0.586 (2.218)	0.000	4.9×10^{-4} (5.2×10^{-4})	0.000	0.000	0.000	0.000	0.000 (1.95×10^{-4})	0.000	6.3×10^{-4} (5.20×10^{-4})	0.161 (4.864)	0.000
	R^2 (clay colloid)	0.75	0.87	0.98	0.87	0.95	0.77	NA	0.83	NA	0.71	0.22	0.95
	R^2 (total mobile virus)	0.87	0.6	0.76	0.78	0.89	0.58	0.89	0.79	0.54	0.92	0.65	0.83
	R^2 (free virus)	0.84	NA	NA	0.71	0.74	0.7	0.86	0.53	0.8	0.92	0.65	0.72
	AIC	−815.95	−706.98	−731.89	−943.06	−937.67	−825.51	−655.82	−660.62	−514.75	−900.50	−833.59	−774.6
	AICc	−815.24	−706.63	−731.34	−942.61	−937.16	−825.20	−655.46	−659.63	−514.33	−899.96	−833.13	−774.25
	BIC	−805.96	−702.40	−724.82	−935.46	−930.50	−820.70	−651.32	−651.80	−510.43	−893.39	−826.06	−769.99
Co-transport (one-way coupled model)	k_a'(/min)	2.073 (369.36)	0.017 (0.003)	0.032 (0.003)	0.008 (0.003)	0.010 (0.001)	0.018 (0.001)	0.003 (2.27×10^{-4})	0.012 (0.002)	0.012 (8.31×10^{-4})	0.004 (1.75×10^{-4})	0.007 (0.001)	0.010 (9.21×10^{-4})
	k_d'(/min)	12.157 (2161.54)	0.002 (0.001)	3.5×10^{-4} (0.001)	0.020 (0.008)	0.002 (0.001)	0.000	0.000	0.002 (0.002)	0.000	0.000	0.001 (0.002)	0.000
	R^2 (total mobile virus)	0.84	0.8	0.58	0.74	0.84	NA	0.9	0.61	0.65	0.71	0.4	0.48
	R^2 (free virus)	0.93	0.44	0.43	0.82	0.76	0.73	0.87	0.55	0.8	0.92	0.65	0.73
	AIC	−284.62	−279.0	−274.26	−278.81	−304.16	−267.00	−245.69	−182.62	−202.24	−292.70	−225.34	−234.61
	AICc	−283.62	−277.72	−272.99	−277.76	−303.02	−266.34	−245.12	−181.12	−201.49	−292.13	−224.25	−234.03
	BIC	−281.95	−276.72	−271.98	−276.21	−301.72	−265.73	−244.52	−180.63	−201.30	−291.52	−222.83	−233.43
Co-transport (one-way coupled model): Simulating the clay colloid breakthrough curve	R^2 (clay colloid)	0.46	0.78	NA	NA	0.79	NA	NA	NA	NA	NA	NA	0.39

NA: Not applicable as the fitting is poor.
[a] The standard errors associated with the estimated parameter values are given in parentheses.

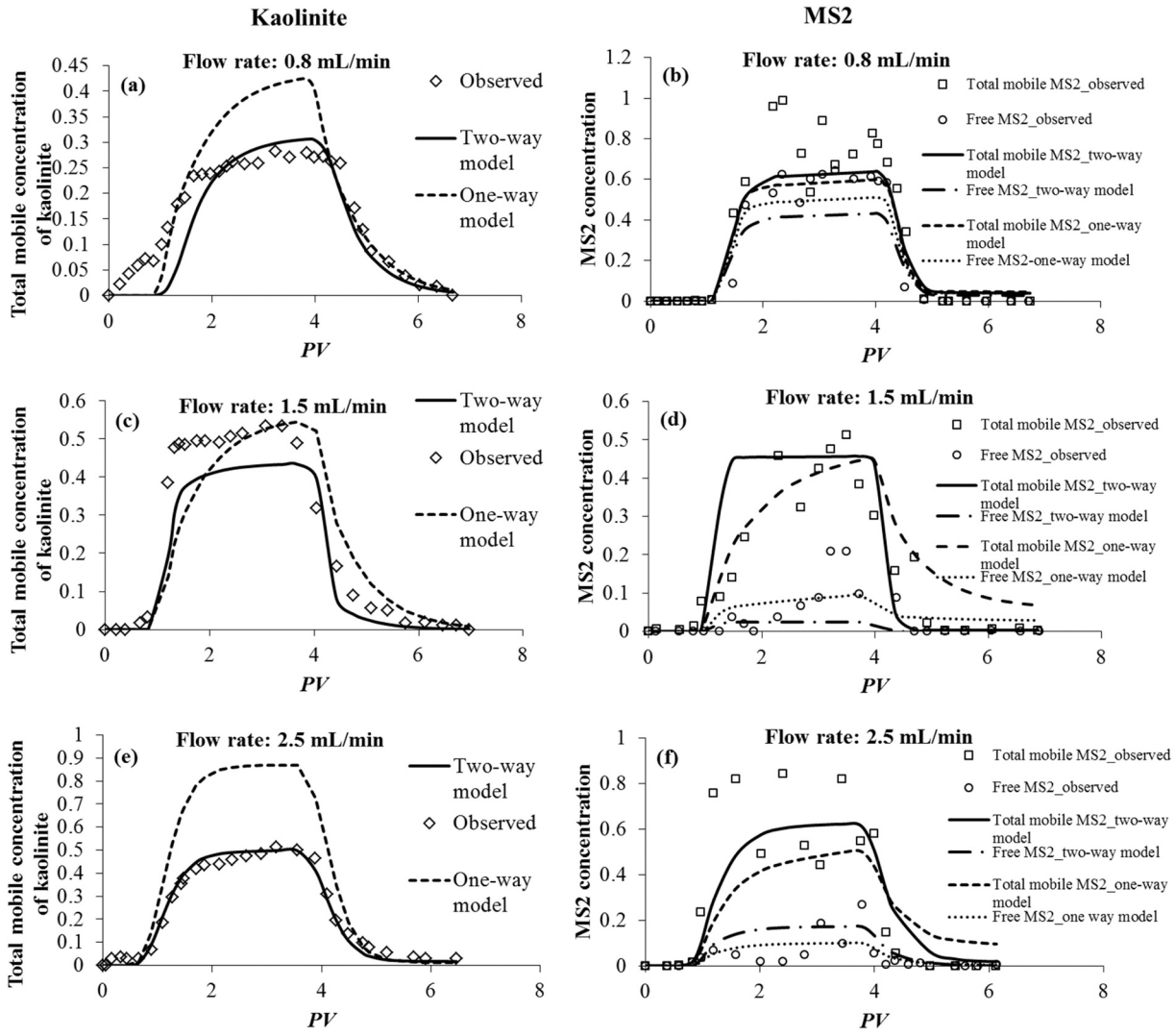

Fig. 8. Observed and fitted breakthrough curves for the co-transport of kaolinite and MS2 (experiments of Syngouna and Chrysikopoulos, 2013): total mobile concentration of kaolinite (a, c, e) and total mobile and free concentrations of MS2 (b, d, f) at flow rates of 0.8 mL/min (a and b), 1.5 mL/min (c and d), and 2.5 mL/min (e and f).

(*agg*) from our study shows similar values for kaolinite and montmorillonite at 2.5 mL/min as the fit is poor for montmorillonite at other flow rates. This is in agreement with the Derjaguin-Landau-Verwey-Overbeek (DLVO) energy profiles for adenovirus interaction with kaolinite and montmorillonite, which have similar values of primary and secondary minima depth for both kaolinite and montmorillonite (Fig. 7). The DLVO energy profile is calculated as the sum of electric double layer energy (Hogg et al., 1966), London van der Waals energy (Gregory, 1981) and Born repulsion energy (Ruckenstein and Prieve, 1976) by assuming a sphere-plate interaction between adenovirus and clay colloids. The values of various parameters used in the calculation are particle radius of adenovirus = 37.5 nm, ionic strength = 1.4 mM, surface potential = −26.03 mV (kaolinite), −20.5 mV (montmorillonite) and − 21.78 mV (adenovirus), temperature = 298 K, Hamaker constant = 3.29×10^{-20} J (adenovirus-water-kaolinite), 2.78×10^{-20} J (adenovirus-water-montmorillonite) and dielectric constant of water = 78.4. The Hamaker constants for adenovirus-water-kaolinite and adenovirus-water-montmorillonite are calculated using the Hamaker constants for adenovirus-water-adenovirus and kaolinite-water-kaolinite (Chrysikopoulos et al., 2017; Kokkinos et al., 2015).

4.4. *Simulating experimental results of Syngouna and Chrysikopoulos (2013)*

Syngouna and Chrysikopoulos (2013) studied the co-transport of clay colloids (kaolinite and montmorillonite) and bacteriophages (MS2 and φx174) in laboratory columns of 2.5 cm in diameter and 30 cm long, packed with glass beads. In our model, clay colloids are colloid 1 and bacteriophages are colloid 2. The dry bulk density of the porous medium was 1.61 g/cm^3 and porosity was 0.42. The hydrodynamic diameters of kaolinite and montmorilonite were 842.85 ± 125.85 nm and 1187 ± 380.81 nm, respectively. The effective particle diameters of MS2 and φx174 were in the range of 24–26 nm, and 25–27 nm, respectively. This study involved twelve co-transport experiments: kaolinite-MS2, montmorillonite-MS2, kaolinite-φx174, and montmorillonite- φx174, each at three different flow rates of 0.8, 1.5 and 2.5 mL/min. Each co-transport experiment involved passing clay colloidal suspension and viral suspension simultaneously into the column for 3 PVs, followed by flushing the column with ddH_2O for 3PVs. Effluent samples were collected at regular intervals and analysed for total clay, free virus, and total mobile virus concentrations.

The deposition of clay colloids and viruses to the solid surface is described by two-site and one-site kinetic models, respectively

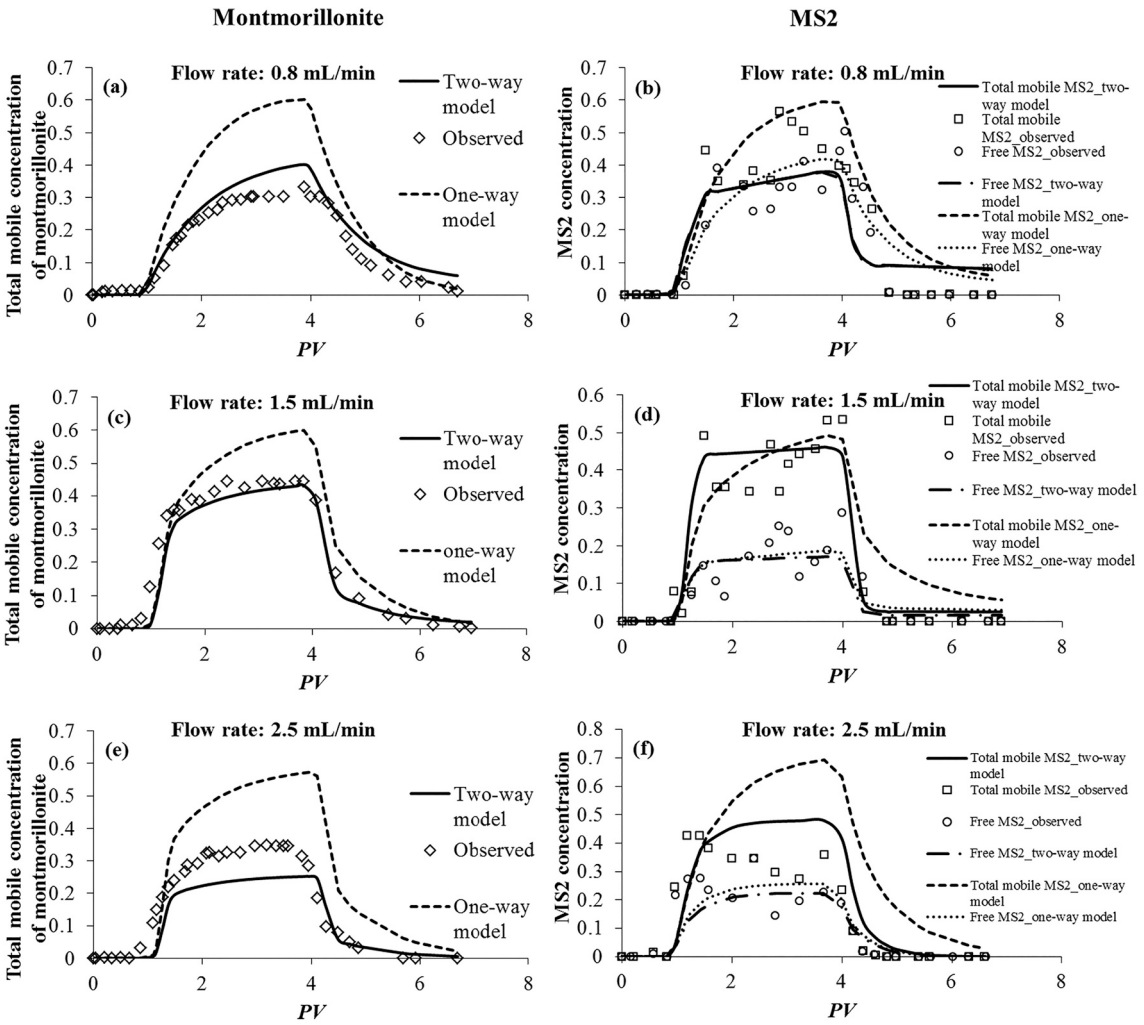

Fig. 9. Observed and fitted breakthrough curves for the co-transport of montmorillonite and MS2 (experiments of Syngouna and Chrysikopoulos, 2013): total mobile concentration of montmorillonite (a, c, e) and total mobile and free concentrations of MS2 (b, d, f) at flow rates of 0.8 mL/min (a and b), 1.5 mL/min (c and d), and 2.5 mL/min (e and f).

(Appendix B). The parameters describing the deposition of viruses and clays to the grain surface during their individual transport are given in Table 1 of Seetha et al. (2015) and are not reproduced here. The deposition parameters estimated using two-way and one-way coupled models are given in Table 3. Figs. 8, 9, 10 and 11 show the observed and fitted breakthrough curves of clays and viruses obtained by using one-way and two-way coupled models for the co-transport of kaolinite-MS2, montmorillonite-MS2, kaolinite- φx174 and montmorillonite-φx174, respectively. The two-way coupled model fits the observed breakthrough curves reasonably well in most of the cases, except for kaolinite data during kaolinite- φx174 co-transport at 0.8 and 2.5 mL/min. It is clear from Figs. 8–11 and Table 3 that the one-way coupled model could not fit the observed breakthrough curves of clay colloids in most of the experiments. The above findings are in line with the values of *AIC*, *AICc*, and *BIC* which favours the two-way coupled model (Table 3). Seetha et al. (2015) followed the procedure that was used by others (Šimunek et al., 2006; Vasiliadou and Chrysikopoulos, 2011) to fit the experimental data of Syngouna and Chrysikopoulos (2013) using a one-way coupled model. But that procedure is contradicting the physics of the one-way coupled model, which assumes that the transport properties of colloid 1 are not affected by the presence of colloid 2 on its surface. The fitted curves and estimated parameter values for the one-way coupled model given in this paper are different from those given in Seetha et al. (2015) for the experiments of Syngouna and Chrysikopoulos (2013) because of the more realistic fitting procedure we followed in this study. Table 3 shows that the rate coefficient of attachment of bacteriophages to clay particles obtained from the two-way coupled model increased with flow rate for all co-transport experiments. Syngouna and Chrysikopoulos (2013) observed a greater value of collision efficiency of MS2 than φx174 to both clays, which is attributed to the hydrophobic nature of MS2 based on the extended DLVO calculations (Chrysikopoulos and Syngouna, 2012). This is consistent with the values of k_a estimated using a two-way coupled model (Table 3) for most of the cases. Also, Syngouna and Chrysikopoulos (2013) noticed that the retention of both viruses were more in the presence of kaolinite than montmorillonite due to more negative hydrophobic interaction energy for kaolinite than montmorillonite for both the viruses (Chrysikopoulos and Syngouna, 2012). This is in line with the estimated values of k_a given in Table 3.

4.5. *Simulating the experimental results of Georgopoulou et al. (2020)*

Georgopoulou et al. (2020) studied the effect of GO nanoparticles on the transport behaviour of *E. coli*, *E. faecalis*, and *S. aureus* through saturated quartz sand by performing laboratory column experiments. The column was 30 cm long and 2.5 cm in diameter. The bulk density

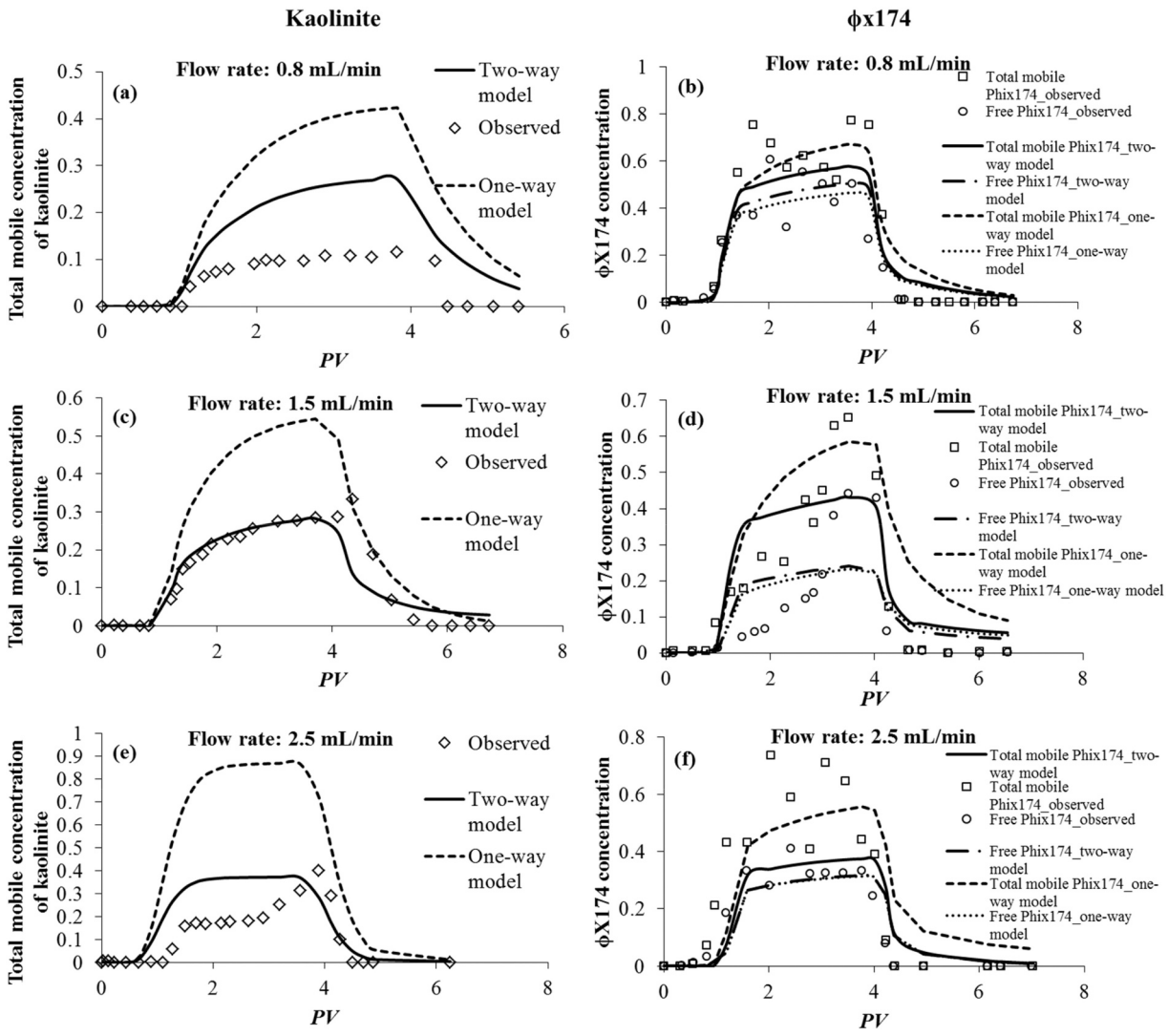

Fig. 10. Observed and fitted breakthrough curves for the co-transport of kaolinite and ϕx174 (experiments of Syngouna and Chrysikopoulos, 2013): total mobile concentration of kaolinite (a, c, e) and total mobile and free concentrations of ϕx174 (b, d, f) at flow rates of 0.8 mL/min (a and b), 1.5 mL/min (c and d), and 2.5 mL/min (e and f).

and porosity of the sand were 1.75 g/cm^3 and 0.39, respectively. Phosphate buffer solution of 2 mM ionic strength at neutral pH was used as the background solution. The hydrodynamic diameters of *E. coli*, *E. faecalis*, *S. aureus*, and GO nanoparticles were 1090.0 ± 62 nm, 1081.9 ± 102.9 nm, 729.9 ± 85.9 nm, and 546.3 ± 43.4 nm, respectively. Both individual and co-transport experiments were conducted at a constant flow rate of 0.8 mL/min. Individual transport experiments consisted of injecting 3 PVs of colloidal suspension of GO nanoparticles or biocolloids into the column, followed by flushing the column with colloid-free background solution for 5 PVs. Each co-transport experiment consisted of injecting 3 PVs of colloidal suspensions of GO nanoparticles and biocolloids simultaneously into the column, followed by flushing the column with colloid-free background solution for 5 PVs.

The interaction of biocolloids with the grain surface is described using a first-order kinetic model whereas the deposition of GO nanoparticles onto the grain surface is described using a first-order kinetic model with blocking (Appendix B). The parameters describing the deposition of biocolloids to the grain surface during their individual transport and the inactivation in aqueous and solid phases, as given in Georgopoulou et al. (2020), are used in our study. Fig. 12 shows the observed and fitted breakthrough curves during the co-transport of *E. coli*-GO, *E. faecalis*-GO, and *S. aureus*-GO. Table 4 gives the values of fitted parameters. The one-way coupled model could not fit the breakthrough curves of *E. coli* and *E. faecalis*, and its performance is poor as compared to the two-way coupled model for the co-transport of *E. coli*-GO (Fig. 12 a,b), and *E. faecalis*-GO (Fig. 12 c,d). This is supported by the model selection criteria (*AIC*, *AICc*, and *BIC*) which indicates that the performance of the two-way coupled model is better than the one-way coupled model (Table 4). Fig. 12e shows that neither the two-way model nor the one-way model could satisfactorily simulate the breakthrough curve of GO nanoparticles during *S. aureus*-GO co-transport. Georgopoulou et al. (2020) found that the presence of GO nanoparticles increased biocolloid retention in the porous medium. This is in line with the estimated values of parameters from the two-way coupled model given in Table 4, which shows that the attachment rate coefficient of heteroaggregation kinetics (k_a) and the heteroaggregate deposition on to the grain surface ($k_{a(agg)}$) are larger than the biocolloid attachment parameter during their individual transport (k_{1cs}). Also, Georgopoulou et al. (2020) found that *E. faecalis* least affected the transport of GO nanoparticles, and GO nanoparticle retention was largest in the presence

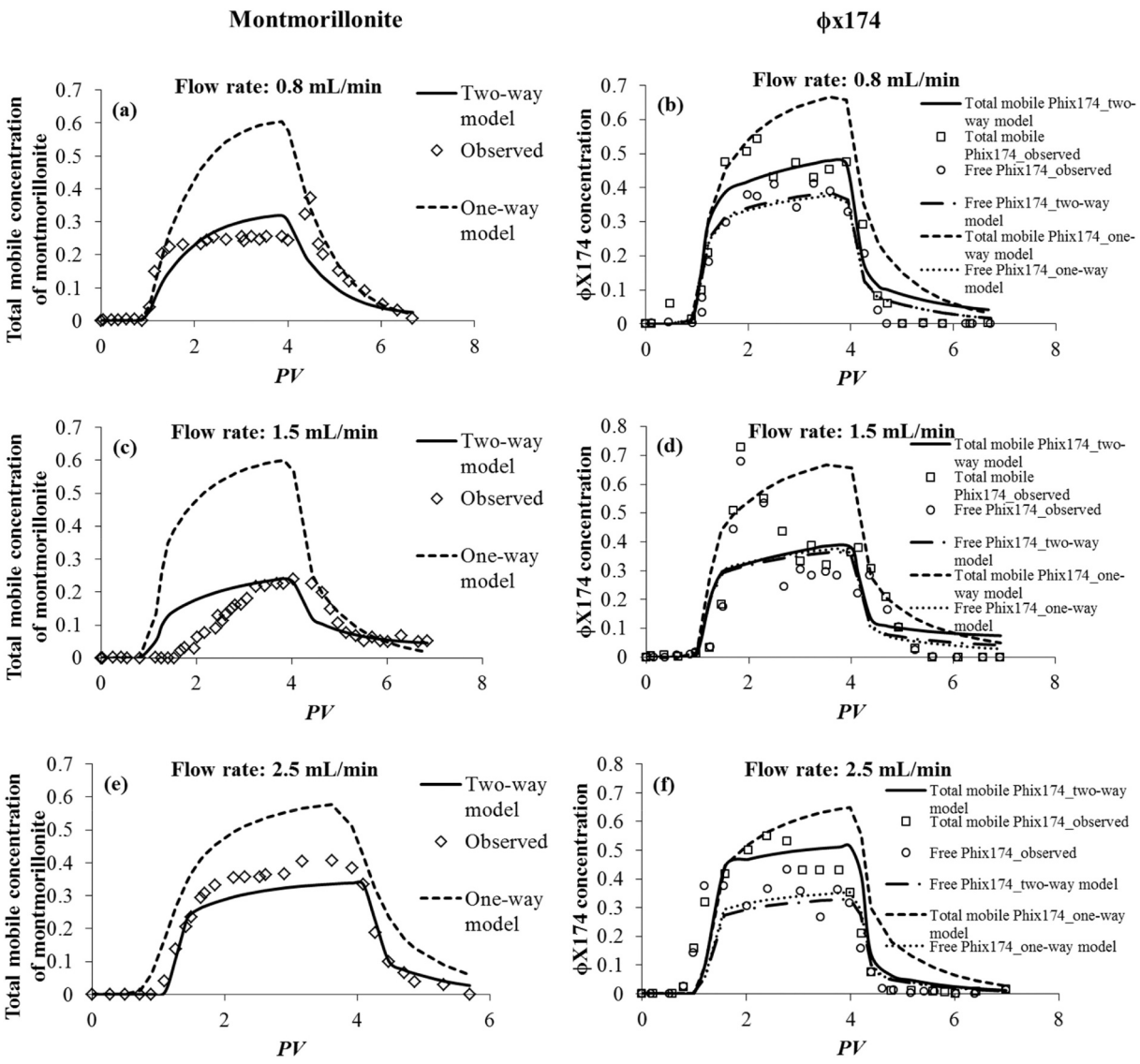

Fig. 11. Observed and fitted breakthrough curves for the co-transport of montmorillonite and ϕx174 (experiments of Syngouna and Chrysikopoulos, 2013): total mobile concentration of montmorillonite (a, c, e) and total mobile and free concentrations of ϕx174 (b, d, f) at flow rates of 0.8 mL/min (a and b), 1.5 mL/min (c and d), and 2.5 mL/min (e and f).

of *S. aureus*. The estimated parameter values from the two-way coupled model (Table 4) are consistent with this observation, which shows the value of $k_{a(agg)}$ being smallest in the presence of *E. faecalis* and largest in the presence of *S. aureus*. Also, the value of k_a/k_d is smallest in the presence of *E. faecalis* and the kinetics of heteroaggregation is irreversible in case of *S. aureus*. This is supported by the extended DLVO energy calculations given in Georgopoulou et al. (2020), which shows that GO-*E. faecalis* interaction has the smallest secondary minimum and largest energy barrier and GO-*S. aureus* has the largest secondary minimum depth and smallest energy barrier. Hence, GO nanoparticles will have less attachment to *E. faecalis* compared to *S. aureus*. Since, *E. faecalis*-sand interaction has the least hydrophobic energy and largest energy barrier, and *S. aureus*-sand has the largest secondary minimum depth and lowest energy barrier, the heteroaggregates of GO- *E. faecalis* and GO-*S. aureus* may also behave similarly. This implies that the deposition kinetics of heteroaggregates to the grain surface and kinetics of heteroaggregate formation play a dominant role in controlling the transport of GO nanoparticles in the presence of biocolloids. Moreover, Georgopoulou et al. (2020) observed from mass recovery data and the calculated collision efficiencies that in the presence of GO nanoparticles, *E. coli* has the largest collision efficiency and hence the greatest affinity to adsorb to GO nanoparticles, and *S. aureus* has the least affinity. This is in line with the estimated values of parameters given in Table 4 for a two-way coupled model, which indicates that the ratio of rate coefficients of heteroaggregation (k_a/k_d) and heteroaggregate attachment rate coefficient to the solid surface ($k_{a(agg)}$) for biocolloids being largest for *E. coli* as compared to the corresponding rate coefficients during their individual transport (k_{1cs}/k_{1sc}). There is not much difference in the values of $k_{a(agg)}$ and k_{1cs} for *S. aureus*, and hence its transport is least affected in the presence of GO nanoparticles.

5. Discussions and conclusions

Experimental observations from literature show that during the concurrent transport of two different colloidal types, the retention rates of both colloids are found to be different compared to when they

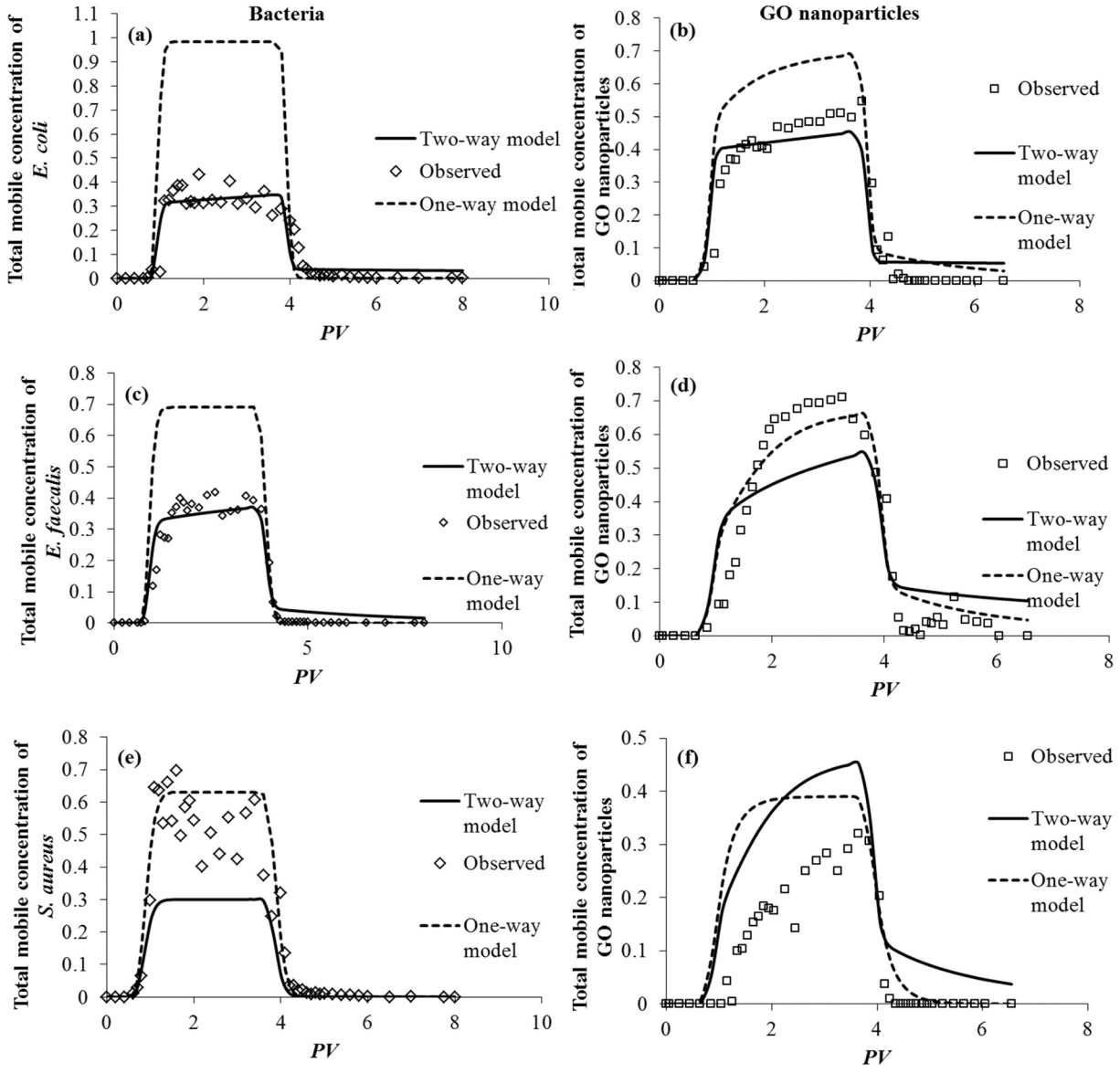

Fig. 12. Observed and fitted breakthrough curves for the co-transport of *E. coli* and GO nanoparticles (a, b), *E. faecalis* and GO nanoparticles (c, d), and *S. aureus* and GO nanoparticles (e, f) (experiments of Georgopoulou et al., 2020): total mobile concentrations of *E. coli* (a), *E. faecalis* (c), *S. aureus* (e) and GO nanoparticles (b, d, f).

undergo transport individually. Thus, the underlying assumption of one-way coupled models, namely the transport of larger colloids not being affected by the presence of smaller colloids, does not agree with observations. This is supported by the results from this study, which show that the one-way coupled model is unable to satisfactorily simulate the observed breakthrough curves of two colloidal types for the co-transport of clay-virus, clay-nanoparticle, and bacteria-nanoparticle. Acceptable fitting of breakthrough curves of the one-way coupled model to observations, for both colloidal types, could be achieved only by assigning different values of deposition parameters than those obtained from their individual transport, as shown by Seetha et al. (2015). Clearly, this violates the assumption of the one-way coupled model that the transport behaviour of larger colloid is unaffected by the presence of the smaller colloid attached to its surface.

The developed two-way coupled model incorporating the first-order heteroaggregation kinetics fits the observed breakthrough curves reasonably well for the co-transport of kaolinite-adenovirus, kaolinite-GO, kaolinite-MS2, kaolinite-φx174, montmorillonite-MS2, montmorillonite- φx174, *E. coli*-GO and *E. faecalis*-GO. It is found that the kinetics of heteroaggregation and the deposition of heteroaggregates to the grain surface control the co-transport of two different colloids. There are two major difficulties with the fitting that we did. First, the data show a lot of scattering, which makes any fitted curve unable to match much of the data. Another issue is that as we fit simultaneously the breakthrough curves of two different colloids, it is difficult to get a satisfactory fitting for some cases for a two-way coupled model. The model selection criteria such as *AIC*, *AICc* and *BIC* favours the two-way coupled model over the one-way coupled model for the experimental data considered in this study. We found that the two-way model is not capable of simulating the experimental results during the co-transport of montmorillonite–adenovirus, and *S. aureus*-GO. The major limitation of the developed model is that it is applicable only to the cases in which the retention of both the colloidal types either increase or decrease during the co-transport as compared to their individual transport behaviour. The model output will be useful in predicting the travel distance of colloidal contaminants such as viruses, bacteria, and engineered nanoparticles in groundwater in the presence of natural colloids such as clays and bacteria. This information in turn is essential to estimate the safe location of drinking water wells from the source of contamination.

Table 4
Fitted parameters using two-way and one-way coupled models for the experimental results of Georgopoulou et al. (2020)[a].

Bacteria			*E. coli*	*E. faecalis*	*S. aureus*
Individual transport	GO nanoparticles	k_{2cs} (/min)	0.017 (0.003)	0.017 (0.003)	0.017 (0.003)
		k_{2sc} (/min)	0.007 (0.003)	0.007 (0.003)	0.007 (0.003)
		s_{2max} (mg/mg)	2.76 × 10^{-6} (4.02 × 10^{-7})	2.76 × 10^{-6} (4.02 × 10^{-7})	2.76 × 10^{-6} (4.02 × 10^{-7})
		R^2	0.93	0.93	0.93
Co-transport (two-way coupled model)		k_a (/min)	1.349 (0.823)	0.023 (0.005)	0.006 (0.007)
		k_d (/min)	0.001 (2.49 × 10^{-4})	0.002 (0.001)	0.000
		$k_{a(agg)}$ (/min)	0.006 (6.81 × 10^{-4})	0.002 (0.001)	0.097 (1.13)
		$k_{d(agg)}$(/min)	0.000	0.000	0.000
		R^2 (bacteria)	0.87	0.94	0.57
		R^2 (GO)	0.88	0.79	0.55
		AIC	−964.79	−840.55	−669.57
		AICc	−964.31	−840.07	−669.29
		BIC	−957.32	−833.08	−664.59
Co-transport (one-way coupled model)		k_a' (/min)	0.012 (0.006)	0.003 (3.61 × 10^{-4})	5.303 (524.42)
		k_d' (/min)	0.000	0.000	0.000
		R^2 (GO)	0.56	0.89	NA
		AIC	−335.06	−415.09	−343.77
		AICc	−334.76	−414.79	−343.47
		BIC	−333.30	−413.33	−342.01
Co-transport (one-way coupled model): Simulating the bacteria breakthrough curve		R^2 (bacteria)	NA	NA	0.87

NA: Not applicable as the fitting is poor.
[a] The standard errors associated with the estimated parameter values are given in parentheses.

Nomenclature

c_1 Mass Concentration of colloid 1 in the aqueous phase $\left[\frac{M}{L^3}\right]$

c_{10} Inlet concentration for the free form of colloid 1 $\left[\frac{M}{L^3}\right]$

c_2 Mass concentration of colloid 2 in aqueous phase $\left[\frac{M}{L^3}\right]$

c_{20} Inlet concentration for the free form of colloid 2 $\left[\frac{M}{L^3}\right]$

c_3 Mass concentration of heteroaggregates in the aqueous phase $\left[\frac{M}{L^3}\right]$

c Model fitted concentration of tracer $\left[\frac{M}{L^3}\right]$

c_{obs} Eperimentally measured concentration of tracer $\left[\frac{M}{L^3}\right]$

c_{1obs} Experimentally measured concentration of colloid 1 from individual transport experiments $\left[\frac{M}{L^3}\right]$

c_{2obs} Experimentally measured concentration of colloid 2 from individual transport experiments $\left[\frac{M}{L^3}\right]$

$c_{colloid1obs}$ Experimentally measured total mobile concentration of colloid 1 from co-transport experiments $\left[\frac{M}{L^3}\right]$

$c_{colloid2obs}$ Experimentally measured total mobile concentration of colloid 2 from co-transport experiments $\left[\frac{M}{L^3}\right]$

$D_L{}^1$ Dispersion coefficient of colloid 1 $\left[\frac{L^2}{T}\right]$

$D_L{}^2$ Dispersion coefficient of colloid 2 $\left[\frac{L^2}{T}\right]$

k_{1cs} Rate coefficient for attachment of colloid 1 to grain surface for a one-site kinetic model $\left[\frac{1}{T}\right]$

k_{1sc} Rate coefficient for detachment of colloid 1 from grain surface for a one-site kinetic model $\left[\frac{1}{T}\right]$

k_{11cs} Rate coefficient for attachment of colloid 1 to site 1 for a two-site kinetic model $\left[\frac{1}{T}\right]$

k_{11sc} Rate coefficient for detachment of colloid 1 from site 1 for a two-site kinetic model $\left[\frac{1}{T}\right]$

k_{12cs} Rate coefficient for attachment of colloid 1 to site 2 for a two-site kinetic model $\left[\frac{1}{T}\right]$

k_{2cs} Rate coefficient for attachment of colloid 2 at grain surface for a one-site kinetic model $\left[\frac{1}{T}\right]$

k_{2sc} Rate coefficient for detachment of colloid 2 from grain surface for a one-site kinetic model $\left[\frac{1}{T}\right]$

k_{21cs} Rate coefficient for attachment of colloid 2 to site 1 for a two-site kinetic model $\left[\frac{1}{T}\right]$

k_{21sc} Rate coefficient for detachment of colloid 2 from site 1 for a two-site kinetic model $\left[\frac{1}{T}\right]$

k_{22cs} Rate coefficient for attachment of colloid 2 to site 2 for a two-site kinetic model $\left[\frac{1}{T}\right]$

k_a Rate coefficient for attachment of colloid 1 to colloid 2 and vice versa for two-way coupled model $\left[\frac{1}{T}\right]$

k_d Rate coefficient for detachment of colloid 1 from colloid 2 and vice versa for two-way coupled model $\left[\frac{1}{T}\right]$

$k_{a(agg)}$ Rate coefficient for attachment of heteroaggregates to grain surface $\left[\frac{1}{T}\right]$

$k_{d(agg)}$ Rate coefficient for detachment of heteroaggregates from grain surface $\left[\frac{1}{T}\right]$

k_a' Rate coefficient for attachment of colloid 2 to colloid 1 for one-way coupled model $\left[\frac{1}{T}\right]$

k_d' Rate coefficient for detachment of colloid 2 from colloid 1 for one-way coupled model $\left[\frac{1}{T}\right]$

k_B Boltzmann constant [$ML^2T^{-2}K^{-1}$]

L Length of the porous medium domain

obs number of observations

[-] P number of model parameters estimated [-]

s_1 Concentration of colloid 1 adsorbed to grain surface $\left[\frac{M}{M}\right]$

s_2 Concentration of colloid 2 attached to grain surface $\left[\frac{M}{M}\right]$

s_3 Mass concentration of heteroaggregates adsorbed at the grain surface $\left[\frac{M}{M}\right]$

s_{11} Concentration of colloid 1 attached to site 1 for a two-site kinetic model $\left[\frac{M}{M}\right]$

s_{12} Concentration of colloid 1 attached to site 2 for a two-site kinetic model $\left[\frac{M}{M}\right]$

s_{21} Concentration of colloid 2 attached to site 1 for a two-site kinetic model $\left[\frac{M}{M}\right]$

s_{22} Concentration of colloid 2 attached to site 2 for a two-site kinetic model $\left[\frac{M}{M}\right]$

s_m Mass of colloid 2 per unit mass of heteroaggregates in aqueous phase $\left[\frac{M}{M}\right]$

s_{im} Mass of colloid 2 per unit mass of heteroaggregates at grain surface $\left[\frac{M}{M}\right]$

s_{2max} Maximum adsorption capacity of the grain surface for colloid 2 $\left[\frac{M}{M}\right]$

v_1 Pore-water velocity of colloid 1 $\left[\frac{L}{T}\right]$

v_2 Pore-water velocity of colloid 2 $\left[\frac{L}{T}\right]$

t_{in} Duration of input pulse for colloid 1 and colloid 2 [T]

ϕ interaction energy between particle and grain surface [ML^2T^{-2}]

T Temperature [K]

μ_l Inactivation rate coefficient of colloid 1 in the aqueous phase $\left[\frac{1}{T}\right]$

μ_s Inactivation rate coefficient of colloid 1 at the grain surface $\left[\frac{1}{T}\right]$

ρ_b Bulk density of soil $\left[\frac{M}{L^3}\right]$

θ Porosity of soil [−]

σ^2 Sum of squared residuals divided by the number of observations

Declaration of Competing Interest

The authors declare that they have no known competing financial interests or personal relationships that could have appeared to influence the work reported in this paper.

Acknowledgements

The first author acknowledges the funding received from Department of Science and Technology (sanction no. DST/NM/TAP-AGRI/03/2019(G) IIT Delhi), Government of India. The second author wishes to thank the German Research Foundation (DFG) for supporting this work by funding - EXC2075 – 390740016 under Germany's Excellence Strategy, and acknowledge the support by the Stuttgart Center for Simulation Science (SimTech).

Appendix A. One-way coupled model

Fig. A1 shows the various forms of colloids and the interactions among colloids and with grain surface. Colloid 1 can exist in two different forms: mobile colloids in aqueous phase and immobile colloids attached to grain surface. Colloid 2 can exist in four different forms: free colloids in aqueous phase, immobile colloids attached to grain surface, attached to colloid 1 in aqueous phase, and attached to colloid 1 present at grain surface. The model assumes that the presence of colloid 2 attached onto the surface of colloid 1 does not affect the transport properties of colloid 1, and hence, the transport equations of colloid 1 are decoupled from that of colloid 2 and are solved first at every time step followed by solving the transport equations of colloid 2.

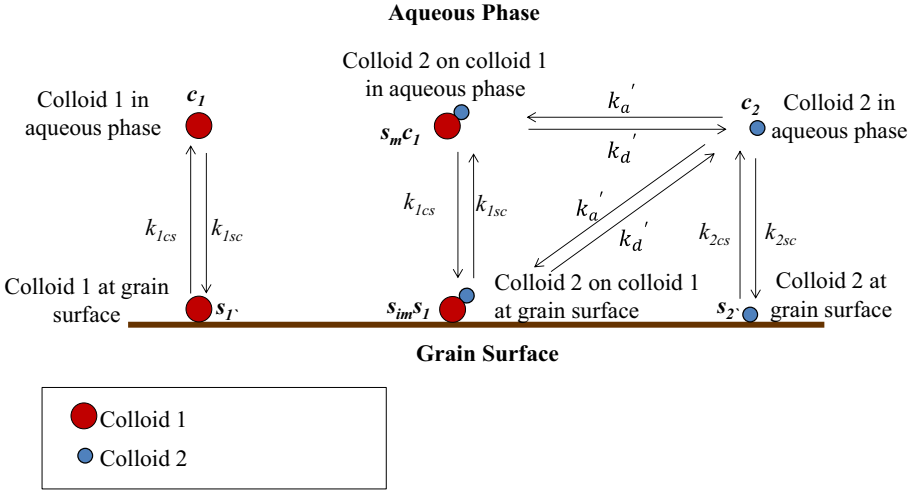

Fig. A1. Conceptual representation of various interactions among colloids and grain surface in porous media for a one-way coupled model (Seetha et al., 2015).

The governing equation for colloid 1 in aqueous phase is given by

$$\theta\frac{\partial c_1}{\partial t}+\rho_b\frac{\partial s_1}{\partial t}=\theta D_L\frac{\partial^2 c_1}{\partial z^2}-v\theta\frac{\partial c_1}{\partial z}-\mu_l\theta c_1-\rho_b\mu_s s_1 \tag{A1}$$

The deposition of colloid 1 to the grain surface is described using either Eqs. (2) or (3). The governing equation for the transport of colloid 2 in

aqueous phase is given by Eq. (4). The deposition of colloid 2 to the grain surface is described using Eqs. (5), (6) or (7).

The mass balance equations for colloid 2 attached to colloid 1 in aqueous phase for colloid 1 undergoing one-site kinetic sorption (Eq. (A2)) or two-site kinetic sorption (Eq. (A3)) are given by

$$\theta\frac{\partial(s_m c_1)}{\partial t} = \theta D\frac{\partial^2(s_m c_1)}{\partial z} - v\theta\frac{\partial(s_m c_1)}{\partial z} + k_a{}' c_2\theta - k_d{}'\theta(s_m c_1) - k_{1cs}\theta(s_m c_1) + k_{1sc}\rho_b(s_{im}s_1) \tag{A2}$$

$$\theta\frac{\partial(s_m c_1)}{\partial t} = \theta D\frac{\partial^2(s_m c_1)}{\partial z} - v\theta\frac{\partial(s_m c_1)}{\partial z} + k_a{}' c_2\theta - k_d{}'\theta(s_m c_1) - k_{11cs}\theta(s_m c_1) + k_{11sc}\rho_b(s_{im}s_{11}) - k_{12cs}\theta(s_m c_1) \tag{A3}$$

The mass balance equations for colloid 2 attached to colloid 1 at grain surface for colloid 1 undergoing one-site kinetic sorption (Eq. (A4)) or two-site kinetic sorption (Eqs. (A5.1)–(A5.3)) are given by.

$$\rho_b\frac{\partial(s_{im}s_1)}{\partial t} = k_a{}' c_2\theta - k_d{}'\rho_b(s_{im}s_1) + k_{1cs}\theta(s_m c_1) - k_{1sc}\rho_b(s_{im}s_1) \tag{A4}$$

$$\rho_b\frac{\partial(s_{im}s_{11})}{\partial t} = k_a{}' c_2\theta - k_d{}'\rho_b(s_{im}s_{11}) + k_{11cs}\theta(s_m c_1) - k_{11sc}\rho_b(s_{im}s_{11}) \tag{A5.1}$$

$$\rho_b\frac{\partial(s_{im}s_{12})}{\partial t} = k_a{}' c_2\theta - k_d{}'\rho_b(s_{im}s_{12}) + k_{12cs}\theta(s_m c_1) \tag{A5.2}$$

Appendix B. Governing equations for the individual transport of colloids

The individual transport of colloid 1 is described by the following equation:

$$\theta\frac{\partial c_1}{\partial t} + \rho_b\frac{\partial s_1}{\partial t} = \theta D_L{}^1\frac{\partial^2 c_1}{\partial z^2} - v_1\theta\frac{\partial c_1}{\partial z} - \mu_l\theta c_1 - \rho_b\mu_s s_1 \tag{B1}$$

The deposition of colloid 1 to the grain surface is described using either a one-site (Eq. (2)) or a two-site kinetic model (Eq. (3)).

The individual transport of colloid 2 is described by the following equation:

$$\theta\frac{\partial c_2}{\partial t} + \rho_b\frac{\partial s_2}{\partial t} = \theta D_L{}^2\frac{\partial^2 c_2}{\partial z^2} - v_2\theta\frac{\partial c_2}{\partial z} \tag{B2}$$

The governing equation for the deposition of colloid 2 at grain surface is described either using a one-site reversible kinetic model without blocking (Eq. (5)), one-site reversible kinetic model with blocking (Eq. (6)), or a two-site kinetic model with site 1 being reversible and site 2 being irreversible (Eq. (7)).

References

Bayat, A.E., Junin, R., Mohsin, R., Hokmabadi, M., Shamshirband, S., 2015. Influence of clay particles on Al_2O_3 and TiO_2 nanoparticles transport and retention through limestone porous media: measurements and mechanisms. J. Nanopart. Res. 17 (219), 1–14.

Cai, L., Tong, M., Ma, H., Kim, H., 2013. Cotransport of titanium dioxide and fullerene nanoparticles in saturated porous media. Environ. Sci. Technol. 47 (11), 5703–5710.

Cai, L., Tong, M., Wan, X., Kim, H., 2014. Influence of clay particles on the transport and retention of titanium dioxide nanoparticles in quartz sand. Environ. Sci. Technol. 48, 7323–7332.

Cai, L., Peng, S., Wu, D., Tong, M., 2016. Effect of different-sized colloids on the transport and deposition of titanium dioxide nanoparticles in quartz sand. Environ. Pollut. 208, 637–644.

Cai, L., He, L., Peng, S., Li, M., Tong, M., 2019. Influence of titanium dioxide nanoparticles on the transport and deposition of microplastics in quartz sand. Environ. Pollut. 253, 351–357.

Chrysikopoulos, C.V., Katzourakis, V.E., 2015. Colloid particle size-dependent dispersivity. Water Resour. Res. 51 (6), 4668–4683.

Chrysikopoulos, C.V., Syngouna, V.I., 2012. Attachment of bacteriophages MS2 and ΦX174 onto kaolinite and montmorillonite: extended-DLVO interactions. Colloids Surf. B: Biointerfaces 92, 74–83.

Chrysikopoulos, C.V., Sotirelis, N.P., Kallithrakas-Kontos, N.G., 2017. Cotransport of graphene oxide nanoparticles and kaolinite colloids in porous media. Transp. Porous Media 119 (1), 181–204.

Dong, Z., Zhang, W., Qiu, Y., Yang, Z., Wang, J., Zhang, Y., 2019. Cotransport of nanoplastics (NPs) with fullerene (C60) in saturated sand: effect of NPs/C60 ratio and seawater salinity. Water Res. 148, 469–478.

Georgopoulou, M.P., Syngouna, V.I., Chrysikopoulos, C.V., 2020. Influence of graphene oxide nanoparticles on the transport and cotransport of biocolloids in saturated porous media. Colloids Surf. B: Biointerfaces 189, 110841.

Gregory, J., 1981. Approximate expressions for retarded van der Waals interaction. J. Colloid Interface Sci. 83 (1), 138–145.

Hogg, R., Healy, T.W., Fuerstenau, D.W., 1966. Mutual coagulation of colloidal dispersions. Trans. Faraday Soc. 62, 1638–1651.

Jin, Y., Pratt, E., Yates, M.V., 2000. Effect of Mineral Colloids on Virus Transport through Saturated Sand Columns, Vol. 29. American Society of Agronomy, Crop Science Society of America, and Soil Science Society of America, pp. 532–539. No. 2.

Katzourakis, V.E., Chrysikopoulos, C.V., 2014. Mathematical modeling of colloid and virus cotransport in porous media: application to experimental data. Adv. Water Resour. 68, 62–73.

Katzourakis, V.E., Chrysikopoulos, C.V., 2015. Modeling dense-colloid and virus cotransport in three-dimensional porous media. J. Contam. Hydrol. 181, 102–113.

Keller, A.A., Sirivithayapakorn, S., Chrysikopoulos, C.V., 2004. Early breakthrough of colloids and bacteriophage MS2 in a water-saturated sand column. Water Resour. Res. 40 (8).

Kokkinos, P., Syngouna, V.I., Tselepi, M.A., Bellou, M., Chrysikopoulos, C.V., Vantarakis, A., 2015. Transport of human adenoviruses in water saturated laboratory columns. Food Environment. Virol. 7 (2), 122–131.

Kumari, J., Mathur, A., Rajeshwari, A., Venkatesan, A., Satyavati, S., Pulimi, M., Chandrasekaran, N., Nagarajan, R., Mukherjee, A., 2015. Individual and co transport study of titanium dioxide NPs and zinc oxide NPs in porous media. PLoS One 10 (8), e0134796.

Li, M., He, L., Zhang, M., Liu, X., Tong, M., Kim, H., 2019. Cotransport and deposition of iron oxides with different-sized plastic particles in saturated quartz sand. Environ. Sci. Technol. 53 (7), 3547–3557.

Li, M., He, L., Zhang, X., Rong, H., Tong, M., 2020. Different surface charged plastic particles have different cotransport behaviors with kaolinite particles in porous media. Environ. Pollut. 267, 115534.

Mahmoudi, D., Rezaei, M., Ashjari, J., Salehghamari, E., Jazaei, F., Babakhani, P., 2020. Impacts of stratigraphic heterogeneity and release pathway on the transport of bacterial cells in porous media. Sci. Total Environ. 729, 138804.

Malakar, A., Snow, D.D., 2020. Nanoparticles as sources of inorganic water pollutants. In: Inorganic Pollutants in Water. Elsevier, pp. 337–370.

Parsai, T., Kumar, A., 2019. Understanding effect of solution chemistry on heteroaggregation of zinc oxide and copper oxide nanoparticles. Chemosphere 235, 457–469.

Qin, Y., Wen, Z., Zhang, W., Chai, J., Liu, D., Wu, S., 2020. Different roles of silica nanoparticles played in virus transport in saturated and unsaturated porous media. Environ. Pollut. 259, 113861.

Ron, C.A., Johnson, W.P., 2020. Complementary colloid and collector nanoscale heterogeneity explains microparticle retention under unfavorable conditions. Environ. Sci. Nano 7 (12), 4010–4021.

Ruckenstein, E., Prieve, D.C., 1976. Adsorption and desorption of particles and their chromatographic separation. AIChE J. 22 (2), 276–283. https://doi.org/10.1002/aic.690220209.

Simunek, J., He, C., Pang, L., Bradford, S.A., 2006. Colloid-facilitated solute transport in variably saturated porous media: numerical model and experimental verification. Vadose Zone J. 5 (3), 1035–1047.
Schijven, J.F., Hassanizadeh, S.M., 2002. Virus removal by soil passage at field scale and ground-water protection of sandy aquifers. Water Sci. Technol. 46 (3), 123–129.
Schijven, J.F., Hoogenboezem, W., Hassanizadeh, M., Peters, J.H., 1999. Modeling removal of bacteriophages MS2 and PRD1 by dune recharge at Castricum, Netherlands. Water Resour. Res. 35 (4), 1101–1111.
Schijven, J.F., Medema, G., Vogelaar, A.J., Hassanizadeh, S.M., 2000. Removal of microorganisms by deep well injection. J. Contam. Hydrol. 44 (3–4), 301–327.
Schijven, J.F., Mülschlegel, J.H.C., Hassanizadeh, S.M., Teunis, P.F.M., de Roda Husman, A.M., 2006. Determination of protection zones for Dutch groundwater wells against virus contamination-uncertainty and sensitivity analysis. J. Water Health 4 (3), 297–312.
Schijven, J.F., Hassanizadeh, S.M., de Roda Husman, A.M., 2010. Vulnerability of unconfined aquifers to virus contamination. Water Res. 44 (4), 1170–1181.
Seetha, N., Kumar, M.S.M., Hassanizadeh, S.M., 2015. Modeling the co-transport of viruses and colloids in unsaturated porous media. J. Contam. Hydrol. 181, 82–101.
Sotirelis, N.P., Chrysikopoulos, C.V., 2017. Heteroaggregation of graphene oxide nanoparticles and kaolinite colloids. Sci. Total Environ. 579, 736–744.
Syngouna, V.I., Chrysikopoulos, C.V., 2013. Cotransport of clay colloids and viruses in water saturated porous media. Colloids Surf. A Physicochem. Eng. Asp. 416, 56–65.
Syngouna, V.I., Chrysikopoulos, C.V., Kokkinos, P., Tselepi, M.A., Vantarakis, A., 2017. Cotransport of human adenoviruses with clay colloids and TiO2 nanoparticles in saturated porous media: effect of flow velocity. Sci. Total Environ. 598, 160–167.
Vasiliadou, I.A., Chrysikopoulos, C.V., 2011. Cotransport of pseudomonas putida and kaolinite particles through water-saturated columns packed with glass beads. Water Resour. Res. 47 (2).
Walshe, G.E., Pang, L., Flury, M., Close, M.E., Flintoft, M., 2010. Effects of pH, ionic strength, dissolved organic matter, and flow rate on the co-transport of MS2 bacteriophages with kaolinite in gravel aquifer media. Water Res. 44 (4), 1255–1269.
Wang, M., Zhang, H., Chen, W., Lu, T., Yang, H., Wang, X., Lu, M., Qi, Z., Li, D., 2021. Graphene oxide nanoparticles and hematite colloids behave oppositely in their co-transport in saturated porous media. Chemosphere 265, 129081.
Yang, H., Tong, M., Kim, H., 2012. Influence of bentonite particles on representative gram negative and gram positive bacterial deposition in porous media. Environ. Sci. Technol. 46 (21), 11627–11634.
Ye, M., Meyer, P.D., Neuman, S.P., 2008. On model selection criteria in multimodel analysis. Water Resour. Res. 44 (3).